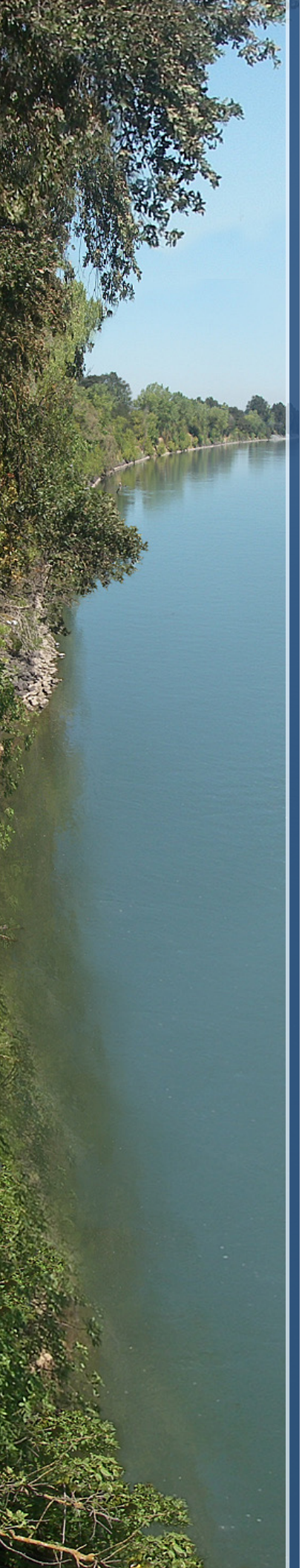

California Levee Vegetation Research Program

Tree Root Architecture – How and where do tree roots grow on and in levees?

Alison M. Berry, PhD and Shih-Ming Chung

Department of Plant Sciences
University of California
Davis, CA 95616

In collaboration with:

- **Gerald Bawden, U.S. Geological Survey, Western Remote Sensing and Visualization Center, Sacramento, CA 95819**
- **Sandra Bond, U.S. Geological Survey, Western Remote Sensing and Visualization Center, Sacramento, CA 95819**
- **Keir Keightley, University of California, Davis**
- **John Lichter, Tree Associates Consulting Arborist**
- **Rune Storesund, Storesund Consulting**
- **Victor Claassen, University of California, Davis**

Sponsoring/Advisory Agencies of the California Levee Vegetation Research Program

California Levee Vegetation Research Program

Tree Root Architecture: How and where do tree roots grow on and in levees?

Alison M. Berry, PhD and Shih-Ming Chung

Department of Plant Sciences
University of California
Davis, CA 95616

Grant funding provided by:
The California Department of Water Resources (Contract No. 4600008761)
and the Sacramento Area Flood Control Agency (Contract No. 986)

25 February, 2013

I. INTRODUCTION

This project was developed to address a key knowledge gap in assessing the impact of trees on levee stability: **Where do tree roots grow in levees?** The project began in 2009, as one component of a research prioritization process by the California Levee Vegetation Research Program (CLVRP) workgroup and California levee managers. The goal of the CLVRP and the CLVRP projects was to provide a scientific basis for management decisions regarding vegetation on levees in the Central Valley of California.

The main target for our excavations was the water-side levee slope, either on the Pocket Levee (Sacramento River, City of Sacramento, CA) or on a levee section in the San Joaquin River National Wildlife Refuge, in Vernalis, CA. We surveyed trees for potential excavation on the land-side of the levee, the water-side, and on riparian banks, during extensive site surveys of several levees, from Yuba City to Vernalis that were organized by Roy Kroll (DWR). Due to several factors, however, all of the tree-root excavations were performed on water-side levee slopes: 1) the importance to levee managers of understanding interactions between tree roots and the levee on the water-side slope; 2) the importance of being able to make comparisons of common sites and species between levees; and 3) because of various site limitations, including environmental regulations, soil removal limitations, etc. It was not possible to excavate trees growing on the riverbanks, for example, both due to environmental regulations, and the practical logistics of soil removal. On the Pocket Levee, trees on the land-side were often quite close to people's homes. We also partially excavated the roots of an over-mature cottonwood tree on the water-side levee slope of the Natomas East Main Drain Canal, Sacramento County, CA.

One initial question was whether different tree species had different root system architectures on levees. In the process of site- and tree- survey and selection, we found that Valley Oak (*Quercus lobata*) and Cottonwood (*Populus fremontii*) were by far the most common native trees capable of growing on levee slopes. Other species initially considered – box elder (*Acer negundo*), willow (*Salix spp.),* etc. – were more riparian than levee-slope trees, and were either not abundant or accessible. Thus, the study focused on Valley Oak and Cottonwood tree root systems, on the water-side levee slope.

Another initial question that the CLVRP prioritized was how the levee tree root systems interacted with soil properties, especially soil compaction. In collaboration with Dr. Vic Claassen, a limited number of soil samples were taken at several depths near two trees on the Vernalis levee, and analyzed for bulk density. It was not possible to make a comprehensive study, but as described in the Discussion (below), the limited study revealed an unusual soil profile due to the constructed nature of the levee.

Because tree root systems are underground, critical parameters of tree root system architecture have been difficult for scientists to determine. Two critical needs were identified for the methodology to be developed for the levee tree project: 1) it was essential to characterize the root systems in precise *in situ* orientation with respect to the levee structure; and 2) it was also important to be able to provide a quantitative basis for the characterization of the root systems. Quantitative data have the capability of being integrated into larger models applicable to levees, such as geotechnical models for seepage and slope stability.

Initially, when we began the project, there were no comprehensive tools for achieving these goals. In 2007, in a preliminary test-excavation on the Mayhew Levee (American River, Sacramento County, CA), we had tested backhoe trenching and Ground-Penetrating Radar as two possible approaches to characterizing tree roots in levees. The backhoe trench profile mapping method was accurate, but limited in scope, since it was not possible to deduce total root architecture from a single trench, or even a series of trenches. Ground Penetrating Radar was not useable on levees, either along the Mayhew Levee, or in later tests in 2010 by the US Army Engineer Research and Development Center (ERDC) on the Pocket Levee, in which we participated as local cooperators. There were too many imaging artifacts due to the conglomerate nature of the soils and levee structures to permit precise interpretation.

For the CLVRP project, we first tested published methods, using pneumatic excavation combined with a Polhemus hand-held 3D digitizing scanning device and a software program created by the research group of Dr. Frederic Danjon (Danjon and Reubens 2008).

The published methods were developed by measuring small trees, but our goal was to excavate larger tree root systems. Although the Polhemus digitizer was useful for small-scale (0.5 m^2) data collection, and was used by ERDC personnel (with our cooperation) on the Pocket Levee for that purpose, we could not use it for whole-root system measurements because we found deviations in detection accuracy at 1-m distances from the target, possibly due to interference from metal content of the soil (iron content; pipes, etc.), or other limitations in the instrument itself for field use. In addition, as a hand-held device, measurement with Polhemus was essentially manual, and particularly challenging to use on complex tree root systems, simply from an accessibility standpoint.

Fortunately, working with Dr. Oliver Kreylos (UC Davis Institute of Data Analysis and Visualization Laboratory), we identified ground-based T-LiDAR as a possible solution to our data collection requirements for the project. In collaboration with Dr. Gerald Bawden, we developed a methodology on a Valley Oak tree in the Pocket Levee, and then used this method of digital data collection for all of the tree root system characterizations. For the excavation phase, we used a heavy-duty version of the pneumatic excavator, because we needed to excavate down to a depth of 2 m to reach the extent of the taproot for some of the levee trees. John Lichter helped to develop a strategy for pneumatic excavation within the levee research context, first used on the Pocket Levee trees, and which we then adapted to the Vernalis site conditions. Numerous student field assistants helped with the excavation process. Dr. Keir Keightley brought ground-based T-LiDAR instruments, courtesy of USGS, to the Vernalis site, and imaged all of the trees excavated on the levee (15 trees on the water-side levee slope); and Dr. Rune Storesund imaged 2 trees on the floodplain flat with his T-LiDAR unit.

Following LiDAR image acquisition, extensive data-processing and conversion to quantitative parameters was required before data could be analyzed and root-system architecture understood. We tested the existing software, AMAPmod (Danjon), and found it to be very difficult to use. Consequently, Shih-Ming Chung, building on the post-processed datasets of Gerald Bawden, Sandra Bond and Keir Keightley, devised an alternative work-flow process using 3D imaging software, the R statistical tools, and software packages for geospatial analysis (see Methods below). In addition, Shih-Ming Chung developed new quantitative models to describe fundamental properties of tree root system architecture and topology. These tools were applied to the analysis of tree

root architecture, biomass distribution, and topology of the levee trees (see Methods, Results, Discussion, below). Both the findings from the study and the models can be incorporated in a range of future analytical contexts, including levee geotechnical modeling applications.

II. METHODS

1. Site Descriptions

1.1 The Pocket levee, Sacramento, CA

Tree root architecture: Valley oak excavation.

The first research site was located on the Pocket Levee, on the east bank of the Sacramento River, Sacramento, California, U.S.A. Two valley oak trees (*Quercus lobata*; 6 meters altitude at a slope angle of 12.37°; latitude 38° 29' 57" N, longitude 121° 33' 28" W) on the waterside (west facing) slope of the levee were chosen for this study (Table 1.1). The altitude of the levee is about 4 m above sea level (m.a.s.l.) at the water line and 10 m.a.s.l. at the levee crest.

The surrounding trees did not substantially shade the target valley oak. Two valley oaks of equivalent size grew to the N and S at a similar position on the levee slope. One large cottonwood (*Populus fremontii*) tree (DBH: 0.84 m; height: 17.45 m; 16.5 m to the West) and one large valley oak (DBH: 1.32 m; height: 18.22 m; 8.3 m to the South) were growing on the lower terrace deposits. The soil particle size distribution of soil samples taken from around the valley oaks, at a depth of approximately 2 feet, was 2% clay/15% silt/83% sand. The bulk density at that depth and location was approximately 1.33 g/cm^3 (data of V. Claassen).

The levee slopes were otherwise covered in grasses, while the levee toe was covered in grasses, shrubs and forbs.

Table 1.1 Properties of target trees excavated, Pocket Levee, Sacramento

Tree ID	Species	Age (year)	Age height (m)*	DBH (m)	Height (m)	Crown area (m^2)
p2009	*Quercus lobata*	34	1.37	0.32	12.98	60
p2010	*Quercus lobata*	36	1.26	0.26	11.04	38.37

* The age height was the tree trunk height at which we measured the tree rings to determine tree age. Actual age is likely 2-5 y greater than ring-width calculation.

Walnut stump excavation. **Do decayed tree roots leave channels that create preferential flow?**

To investigate whether decayed woody root systems typically create hollowed-out structures that could serve as channels leading to internal levee erosion, the root system of a dead walnut tree (a stump) on the Pocket levee was excavated manually, by A.M. Berry with J.M. Lichter and Kyle McKay (ERDC), and the condition of the decayed roots photographed. The walnut stump was located on the land-side of the levee, at approximately the same levee mile as the valley oaks. The stump was one of several stumps and dying trees remaining from a small orchard of walnuts (see Appendix 6).

1.2 San Joaquin River National Wildlife Refuge, Vernalis, CA

A second tree-excavation experiment was conducted in the San Joaquin River National Wildlife Refuge, near Vernalis, California, USA. Trees excavated in the study were located in the riparian zone on the east side of a narrow river bend corridor (San Joaquin River) bounded by farm levees, and extended to the adjacent floodplain. A

valley oak-grassland community occupied the waterside of the flood control levee, with occasional cottonwood, willow, and boxelder trees. The levee site was located at latitude 37° 37' N, and longitude 121° 12' W (Vierra property in RD 2099, Gardner's Cove area), between River Mile 79.00 to River Mile 79.25 of San Joaquin River. The altitude was about six m.a.s.l. at the water line and 10 m.a.s.l. at the levee crest. The levee soil was predominantly a silt-sand loam (approximately 5% clay/55% silt/40% sand). The average bulk density of the soil at about 2 ft depth was 1.63 g/cm^3. Fifteen tree root systems were excavated on the waterside levee slope, which faced northward in an arc along the river bend (from northeast to northwest). Of the fifteen trees, 3 were cottonwoods and 12 were valley oaks. Two control trees (one valley oak and one cottonwood) were excavated, located on the floodplain behind the levee at latitude 37° 36'24" N, and longitude 121° 11'46" W, and 10m.a.s.l. The properties of the trees are given in Table 1.2.

1.3 Natomas, Sacramento County, CA

The third experimental site was located on the levee of the Natomas East Main Drainage Canal, Sacramento County, CA. One very large cottonwood tree (*Populus fremontii*) was selected for evaluating the root system pattern in relation to the levee (Figure 1.3).

Table 1.2 Properties of target trees excavated at RD 2099 Vernalis site.

Tree ID	Species	Age (yr)	Height (m)	DBH (m)	Height (m)	Canopy (m^2)	HSMax**(m)	Rooting Depth (m)
v6	*Populus fremontii*	12	1.28	0.24	9.29	39.63	5.89	1.7
v7	*Populus fremontii*	14	0.14	0.36	9.62	72.98	7.18	2.61
v8	*Quercus lobata*	18	0.82	0.15	5.46	12.79	2.46	1.45
v9	*Quercus lobata*	11	0.87	0.17	5.63	7.86	2.09	1.88
v12	*Populus fremontii*	13	0.15	0.22	7.78	28.83	3.72	1.36
v13	*Quercus lobata*	6	0.42	0.11	4.32	3.10	1.29	1.03
v14	*Quercus lobata*	11	0.81	0.13	4.22	5.31	2.36	1.27
v15	*Quercus lobata*	10	0.38	0.12	3.77	7.71	1.67	1.09
v16	*Quercus lobata*	10	0.3	0.08	3.72	2.87	0.72	0.62
v17	*Quercus lobata*	10	0.36	0.13	4.16	4.93	1.74	1.56
v19	*Quercus lobata*	13	0.07	0.22	NA (Stump)	NA (Stump)	2.87	1.89
v20	*Quercus lobata*	8	0.63	0.16	7.43	10.94	1.63	1.34
v21	*Quercus lobata*	10	0.73	0.13	4.69	6.75	1.75	2.01
v22	*Quercus lobata*	11	0.67	0.16	7.16	10.39	2.16	1.89
v23	*Quercus lobata*	12	0.58	0.21	7.56	29.96	2.69	1.91
vfo	*Quercus lobata*	7	0	0.14	5.6	20.09	2.15	0.66
vfc	*Populus fremontii*	7	0	0.21	7.45	11.21	3.3	1.24

* The age height was the tree trunk height at which we counted the tree rings to determine tree age. Actual age is likely 2-5 y greater than measured. ** HSMax is the maximum horizontal spread of a tree root system.

Figure 1.3. Large, over-mature cottonwood on the water-side levee slope of the Natomas East Main Drainage Canal, before excavation. Note failing branches indicative of internal decay, heavy mistletoe infestation.

The cottonwood tree was located at the levee toe, water-side (4 to 5 m away from the water, latitude 38° 37'01" N, longitude 121° 28'06" W, and 6 m.a.s.l.). The levee was composed of a former agricultural soil (5% clay/52%silt/43%sand), with very similar particle size distribution as the Vernalis site, but with much higher average bulk density at similar depth (average of 1.84g/cm^3 at about 2 feet; data of V. Claassen). Slices of the trunk cross-section were preserved to count annual rings, as well as the largest lateral roots next to the trunk base. Extensive heart-rot decay in the trunk interfered with tree-ring counts. However, 68 rings were counted in cross-section of the largest root collected, so it can be said that the tree was a minimum of 68 years old, and

likely between 68-72 years. The partially-excavated root system was scanned and photographed (Appendix 4).

2. Field Methods

We used a system of excavation and data acquisition that we call the PEALS system: **p**neumatic **e**xcavation **a**nd ground-based tripod **L**iDAR **s**canning. It represents a combination of methods for acquiring in-situ spatial data of tree root systems.

2.1 Pneumatic excavation

Root systems were excavated by pneumatic excavation. This low-disturbance process removed soil with a jet of high-pressure air, revealing the root system. Prior to beginning the excavation, the slope surface was prepared by mowing. The aboveground portion of the tree and the soil surface were surveyed using a ground based Tripod LiDAR (T-LiDAR) laser scanning system. Eventually the aboveground portion of the tree was removed to a height of approximately 1.4 m above the ground, to minimize risk of toppling during the excavation. The soil around target trees/root systems was irrigated overnight to minimize dust and to soften any compacted soil. Soil was then removed using the air knife (Supersonic Air Knife, Model H-XFA) with a high-volume nozzle and 1.5” ID lightweight hose (30m), driven by a 375-cfm air compressor.

2.2 LiDAR scanning system

LiDAR data collection and processing methods. Ground-based T-LiDAR was used to scan the levee soil surface, the aboveground portion of each tree, and the exposed root systems. To acquire LiDAR datasets that could be quantitatively analyzed

in 3-dimension (3D), scans were made from multiple locations around each tree, providing data that could be assembled into 3D visualizations. Collecting data from the bottom surface of the roots was not possible because the roots were scanned in place. To accommodate this limitation, the instrument was positioned close to the soil surface such that as much of the lower surface of the roots was scanned as possible.

Instrumentation: LiDAR data were collected using an Ilris 3D laser scanner (Optech Inc., Vaughan, Ontario, Canada). This instrument is a discrete-return, raster-based scanner with a 1,535 nanometer (nm) laser. The laser beam emitted from the instrument is reflected from the object, and a return signal (e.g. “return”) is collected by the detector. The scanner is battery operated and mounts on a tripod and must be positioned a minimum of three meters from a scanning target. The scanner has a minimum angular step of 0.00115 (degrees) and a 40 (deg) x 40 (deg) field of view. Data were stored on a removable memory card in an Optech proprietary file format.

Pre-excavation scanning: The above ground portion of the tree and the surrounding terrain were scanned prior to excavation to provide a data set describing the coordinates of the terrain prior to disturbance and the size, shape and orientation of the tree canopy and to show the geometry of the trunk with respect to the canopy and soil/levee surface. A minimum of two full-canopy scans were collected for each tree with an additional detailed scan of the trunk and surrounding terrain underneath the canopy.

Tree root scanning: Root system size and complexity varied among the trees scanned. Laser scanner positioning was adapted according to the size of the excavation, complexity of the roots and the shape of the terrain surrounding the excavation. As many as 17 different scans were made for a given tree to properly capture tree root geometry. The distance between the instrument and roots was

maintained at a minimum of three meters but increased to as much as six meters to increase the number of roots in the field of view. Instrument height varied between 0.5 and two meters above the soil surface. As part of the scan collection, each data set contained a single level scan of the tree and surrounding terrain. This level scan was used to provide a reference coordinate system with the z-axis known to be vertical.

Instrument settings: The average distance to the root target was calculated using a pre-scan sampling function of the laser scanner. Using this distance, the scanner adjusted its angular step to keep data density between nine and 16 returns per square centimeter. Scan extent was limited to the roots and other tree features within the scanner field of view. The trunk was scanned multiple times to provide overlapping data for alignment to the pre-excavation canopy data sets.

Repeat scans: Repeat scans of several trees were done to capture root data during and after excavation. This was required on several trees due to the complexity of the roots and the need to remove some of the smaller roots to achieve a more complete excavation of underlying (and obscured) roots. These scanning data sets were collected and processed separately to preserve unique differences between them. In these cases, some roots had altered geometry due to loss of soil support or drying between subsequent (repeat) scans.

Scan data pre-processing: The LiDAR data (called “returns", i.e. the laser signals that return to the detector) are recorded in a spherical coordinate system by the scanner’s detector. The data were converted to a Cartesian coordinate system (xyz) using a software program supplied by Optech. No filtering was done to the data. Laser return intensity was also recorded and stored along with the xyz information. The data were stored in the pif (parametric image format), Innovmetric Software Inc. Quebec City,

Canada. Individual scans were aligned with each other into a master scan, using manual methods followed by alignment in Innometrics Polyworks software. The LiDAR return signals from the exposed soil surfaces below the roots were removed from the data sets to permit better visualization and analysis of the root images.

Coordinate system reorientation: To standardize the spatial reference for analysis of the tree root system data, a master coordinate system for each tree was aligned such that the x-axis was always parallel to the adjacent levee and the y-axis was perpendicular to the x-axis in the horizontal plane. Likewise the data were translated horizontally and vertically to make all x,y,z coordinates positive values.

Data export: Data were then exported to an ASCII text format that included the x, y and z coordinate values as well as the LiDAR return intensity (referred to as xyzi data). For each tree, the data were divided into three groups: all root data plus the soil surface; tree canopy plus soil surface; and roots only.

Ground surface modeling: Pre-excavation scans for each tree were processed to extract points representing the soil surface using Terrascan software (Terrasolid Ltd., Helsinki, Finland). Using a nearest-neighbor analysis, this process selects points that lie at or near the lowest local elevations of the point cloud. These ground point data sets were saved as independent files for the purpose of modeling the surfaces to compare with canopy and sub-soil (root) point distribution.

Root data cleanup: The Keck CAVES facility (Center for Active Visualization in the Earth Sciences) at UC Davis was used to interactively subset the root point cloud data such that all points that did not represent the tree roots were eliminated from the data. The xyzi data were projected in an immersive 3D environment, using the

LiDARViewer tool (Kreylos *et al.*, 2008) which allowed for effective interactive manipulation of the data to best distinguish and select LiDAR returns that represented the tree root surfaces, distinguished from underlying soil, adjacent foliage or instrument noise (points not associated with a physical target).

2.3 Quantitative modeling

2.3.1 Virtual trench profile mapping and tomographic approach

A virtual trench profile (VTP) mapping technique was developed (S-M Chung, unpublished), using methods similar to conventional trench profile mapping (Schuurman & Goedewaagen, 1965; Danjon & Reubens, 2008). The LiDAR data cloud was transformed into parameters for statistical analysis (origin point, root system horizontal spread, image resolution), using the R program and spatial software. The tree root spatial data cloud was then plotted from the 3D point cloud into 2D slices with R tools. As shown in figure 2.3.3.1, virtual trench profiles can be made in any plane, or in multiple planes, and can provide root-cross-sectional data similar to what can be acquired in conventionally-excavated trench profiles. Successive VTPs can be created to measure changes in root morphology or biomass with distance from the tree trunk. Depending on the scale selected, the dataset could represent the biomass of a single root or of a whole tree root system. For example, as shown in figure 2.3.3.2., individual root cross-sections are captured within a single “slice” (equivalent to one trench profile), and can be measured and quantified. These data can be used to create root size classes (not shown), or, of importance to the levee project, to understand the patterns of root depth in relation to soil surface (see figure 3.2.1). At the scale of the whole root system,

successive virtual slices can be made to create a tomographic reconstruction for root system biomass modeling, as discussed below in section 2.3.3.

The centroid function in ArcGIS (version, 9.3.1, Environmental Systems Research Incorporated, Redlands, CA) was used to locate a geometric center of the tree trunk cross-section at the slope surface (abbreviated as TCS). For VTPs representing vertical slices, the TCS point was taken as the origin and the outermost VTP was placed at the horizontal spread point (HSP). For VTPs representing slices of depth, the VTPs were distributed between the highest and lowest measured roots, since the sloping nature of the site meant that some roots in the upslope direction were higher than the TCS.

Accordingly, the VTPs (slices) can be classified as either vertical VTPs or horizontal VTPs in this study. The dimension of the vertical VTPs is defined by the distribution of the root biomass; this varies from the top to the bottom. The dimension of the horizontally-oriented VTPs is defined as the depth*length, where depth is the maximum rooting depth and the length is defined as the $2*\pi*r$ (r is the distance of the VTP to the tree trunk center).

Twenty-four vertical VTPs were created at equal intervals from the TCS to the outermost extent of the roots, so the distance between slices varied depending on the size of the tree being studied. The VTPs were exported in a raster data format and imported into ArcGIS for spatial data transformation (ArcGrid data format). A supervised classification was applied to virtual trench profiles based on the criteria: 0 (root) = gray-scale 0-10; 1 (soil) = gray-scale 11-255, where 0=black and 255=white. Soil and roots were classified in each profile. The spatial metrics processing was computed in the Fragstat spatial pattern analysis program (Mcgarigal et al., 2002). In each virtual trench

profile, the tree root cross-section area (RCSA, cm^2) and root number (RN) were computed as a basis for tree root geometry and biomass analysis.

2.3.2. Key parameters in root system geometry

The data cloud exported from the T-LiDAR scanning provides spatial properties in an ASCII text format. Every point from the data cloud represents its x, y and z coordinate values, which can either form a single tree root system as a relative coordinate system or can be geo-referenced as an open geographic system of coordinates. Consequently, the T-LiDAR data can be used to analyze a single root geometry, scale up to a whole root system behavior, and extend to landscape-level interactions.

Two major properties of the tree root system were chosen to demonstrate how the ultra-high resolution data can build and characterize tree root architecture: root cross-sectional area (RCSA) and the root vector (RV). The RCSA represents the tree root below ground biomass in any soil profile, derived from the virtual trench profiles. RCSA can be used to derive many important root architectural characteristics, such as root volume, root area ratio, and root diameter (Reubens *et al.*, 2007). Virtual trench profiles can be created using the LiDAR technique in any dimension, because it permits digital 3D reconstruction of root systems (see above, 2.3.1, and Fig. 2.3.3.1 as one example).

The second major property, RV (root vector model), is the comprehensive 3D mathematical model representation of the bio- and geo- characteristics of a root system in soil, based on the LiDAR technique of scanning the slope before excavation, then the

aboveground tree, and then roots after soil excavation. Thus the root system can be analyzed in its *in situ* environment (see Section 2.3.4. below). The root system topological characteristics that can be determined from RV data include: the angular and depth relationship of each class of roots to varied surface geomorphology, the root penetration angles, root taper as a function of distance and slope angle, root length/diameter, root curvature, and root branching as a function of distance, slope, and root hierarchy.

2.3.3 RCSA data: Tree root system biomass model and tomographic approach

The RCSA data acquired from virtual trench profile mapping were used to construct root biomass data, using cross-sectional area as a proxy for root biomass. This method can be applied to build a biomass model of the root system, as illustrated in figure 2.3.3.2. As shown in Figure 2.3.3.3, successive tomographic slices sharing the same interval were created in a radial direction from the TCS point, spatially transformed in ArcGrid, and computed in Fragstat to acquire the tree root cross-sectional area (RCSA, cm^2), root number (RN), and soil area (cm^2) on each slice. The maximum horizontal spread from the TCS point was set up as the maximum radius on each tree root system. One tree on the Pocket levee was used as a test-tree for the methods, and 10 trees in the Vernalis levee were analyzed.

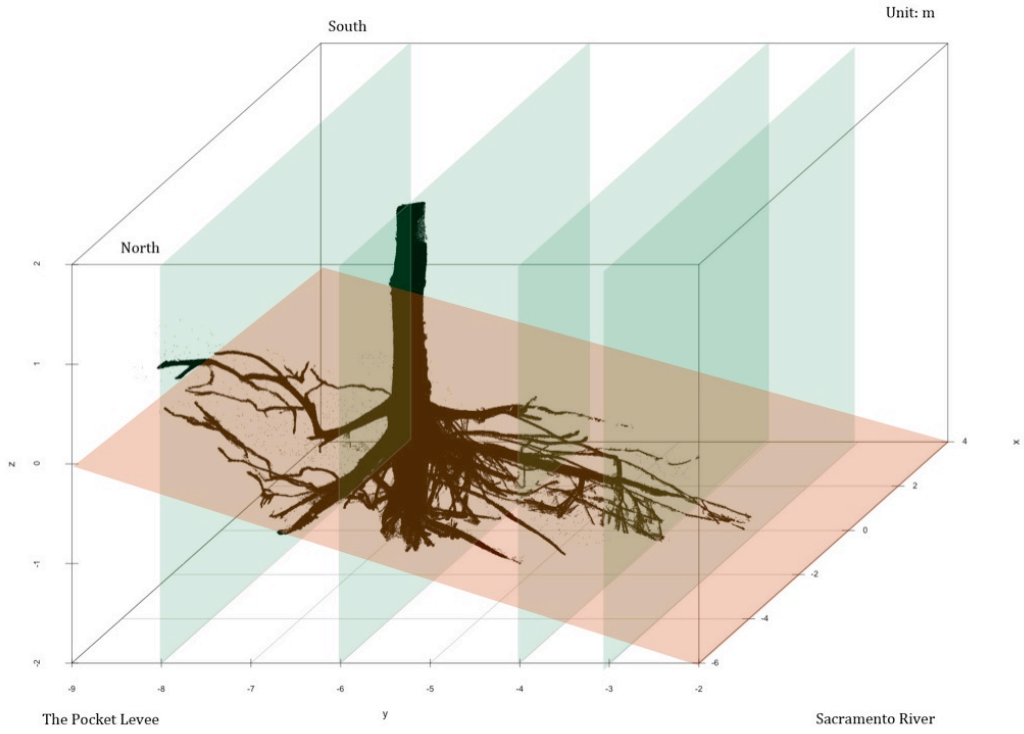

Figure 2.3.3.1. Virtual trench profile as linear tomographic slices in any direction under consideration (Tree ID: p2009). The green slices represent vertical slices.

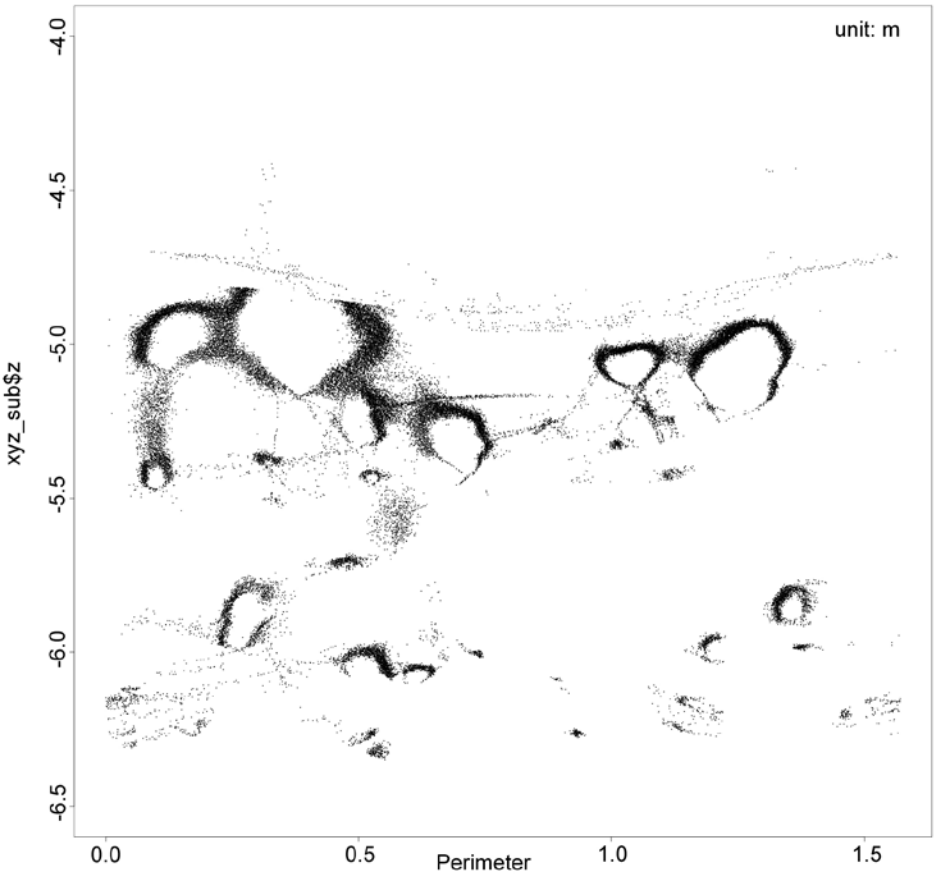

Figure 2.3.3.2. (above) A 3D-to-2D plot of xyz data of a tree root system cross section representing a single tomographic slice, from the oak tree in the Pocket Levee (Tree ID: p2009).

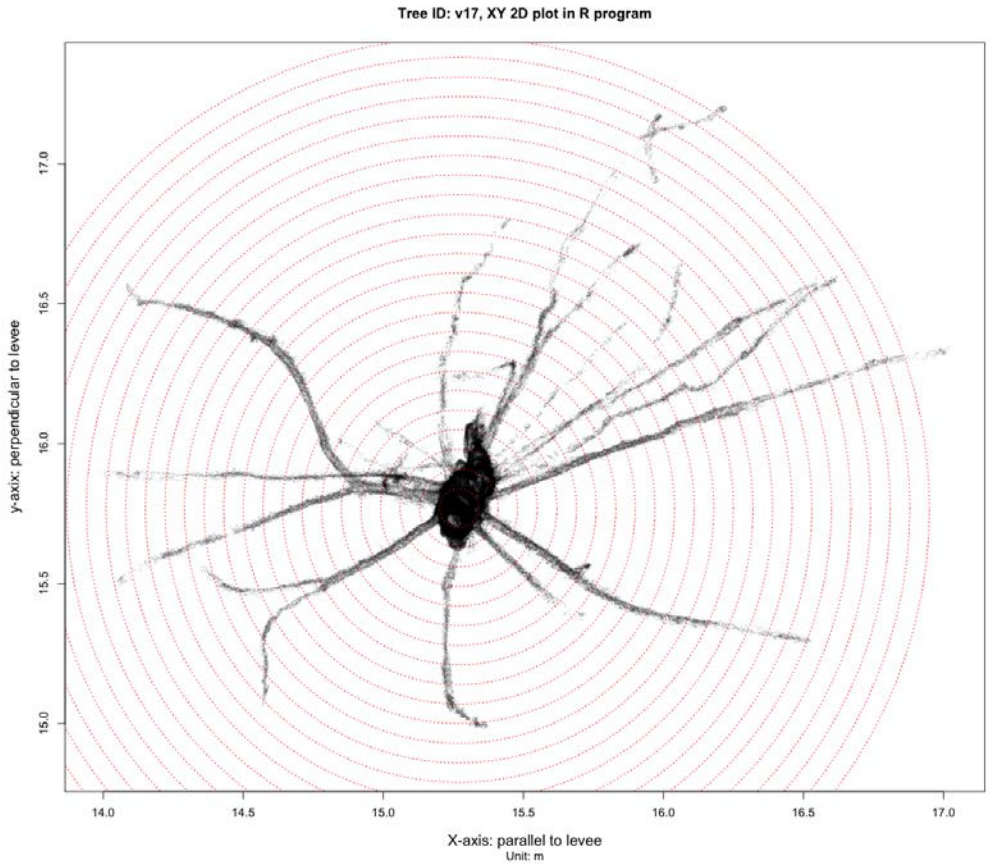

Figure 2.3.3.3. Tomographic slices using spherical coordinates (Tree ID: v17) as a basis for biomass modeling; lines represent successive slices of a tree root system. X-axis: distance of roots in direction parallel to the levee (m); y-axis: distance of roots in direction perpendicular to the levee (m).

2.3.4 Root Vector (RV) data: Tree root system vector model

A vector model to represent three-dimensional directionality of the tree root systems was developed. Vectorization of each T-LiDAR root image was defined by a polyline (sequence of connected vectors) following its path through the center axis of the root in 3D space (figure 2.3.4; generated from root data using the polyline object creator,

Polyworks). Vectors were fit to roots, and edited for accurate biological representation, so that the resulting vector network represented a natural root hierarchy, with first order roots extending to a single termination; secondary roots attaching to the primary roots; tertiary roots to the secondary roots; and so forth. Vector orientation was standardized such that the vector initiated from its distal location and terminated at its proximal location.

The vector data for major structural roots were used to build a root vector model, established by measurement of root length, locus of branch attachment, and a set of angles as shown in table 2.3.4.

Table 2.3.4 Variables of the root vector model

Root ID	Root order	Root Length	Azimuth Angle	Zenith Angle	Branching Angle	Root-Slope Angle	*Root Type
n	n	m	Degree (˚)	Degree (˚)	Degree (˚)	Degree (˚)	H, V, O

*Root types were classified in three categories: horizontal roots (H: angle to soil surface less than 30˚), vertical roots (V: angle to soil surface greater than 60˚), and oblique (O: angle to soil surface >30˚ and <60˚).

At the whole root system scale, the resulting vector model was used to characterize the interaction between slope angle (i.e. angle of the slope soil surface, as measured from the LiDAR data) and root architectural characteristics: in other words, how does the root system grow, in relation to the slope? Do tree roots plunge deeply into the middle of the levee, or does the root system grow in relation to the soil surface?

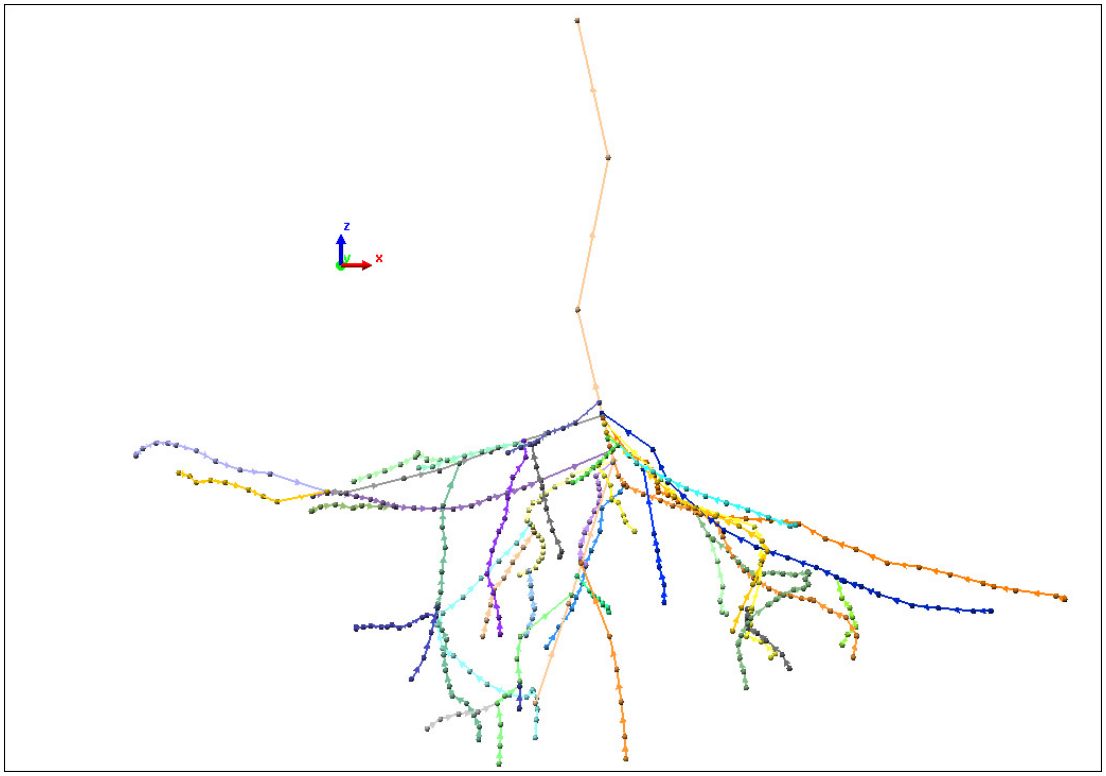

Figure 2.3.4. The vectorization of a tree root system (Tree ID: v08).

2.4 Parametrical Approach

2.4.1 Application of vector modeling to key parameters in tree root system topology

The vector model (table 2.3.4) was used to demonstrate the root system branching pattern of the valley oak tree from the Pocket Levee at different scales. At the single tree scale we classified the whole root system into eight sectors (Figure 2.4.3), and counted root numbers at different topological orders. Topological indices (as defined by Oppelt et al. 2001) were also acquired from the vector model table. We calculated exterior links (v_0), topological depth (a), mean topological depth (b), and the topological

indices (q_a and q_b). According to Oppelt et al. (2001), the topological indices (TI) range from 0 to 1, representing the root branching pattern from “dichotomous” (TI<0.5) to “herringbone”. We further defined the root branching pattern as dichotomous if TI < 0.5 and herringbone if TI > 0.5 for a given tree. Topological indices were determined for whole root systems and for the second-order roots in different directions of the slope (upslope/downslope).

2.4.2 Application of Root Cross Sectional Area (RCSA) and Root Vector (RV) models to characterize tree root architectural traits

Root biomass distribution and spatial configuration. Based on the tomographic reconstruction, root spatial configuration can be derived by using the RCSA from tomographic slices as a proxy at different levels, representing a single root or the whole tree root system. The RCSA of each root at a single root scale and the sum of biomass of all the roots intersected within one slice (RCSA/slice) in a single virtual trench profile (VTP) map (i.e. slice as defined in section 2.3.1) were computed and prepared for analysis. Tomographic slices provided the basis for statistical models with spatial distribution implications, since the extent of the sectional images (slices) ran radially from the TCS point to the furthest root extent. In this study, three major axes, (i.e., x-axis: parallel to the levee line, y-axis: along the slope direction toward the river, and z-axis: the vertical direction) were established for measuring the tomographic extent. Root biomass distribution was calculated along the three major axes.

Horizontal spread and rooting depth. The 3D T-LiDAR data were plotted into 2D planes from two perspectives (i.e., bird’s eye and profile) to acquire the horizontal

spread and the maximum rooting depth of each root system. Four horizontal spread points (i.e., HSXL, HSXR, HSYL, and HSYR) from the bird's eye view perspective were acquired.

In addition, the depth of each root and root system was derived from the tomographic slices. The depth of each root was determined by the distance from the root centroid to the slope surface, using ArcGIS functions.

Branching pattern and rooting angle. Based on the essential root directionality variables acquired in the vector model, relationships among roots could be computed. Topological indices (q_a) were acquired by calculating exterior links (v_0) and topological depth (a) (Oppelt *et al.*, 2001). Topological indices of the whole root system and second-order roots in the two slope directions (upslope/downslope) were acquired.

2.4.3 Symmetry/asymmetry of tree root system architecture

The tree root system was divided into eight sectors for symmetry analysis (figure 2.4.3). We defined the *parallel zone* as the zone in which roots were mainly in a parallel position to the levee, i.e. in sectors 1, 4, 5, and 8 (PRL Zone); and the *perpendicular zone* as the zone in which roots were mainly perpendicular to the levee slope, i.e. in sectors 2, 3, 6, and 7 (PDL Zone). Root number, root biomass distribution, the average rooting depth, and variables of branching pattern and rooting angle were calculated to compare along the major structural axes in both zones.

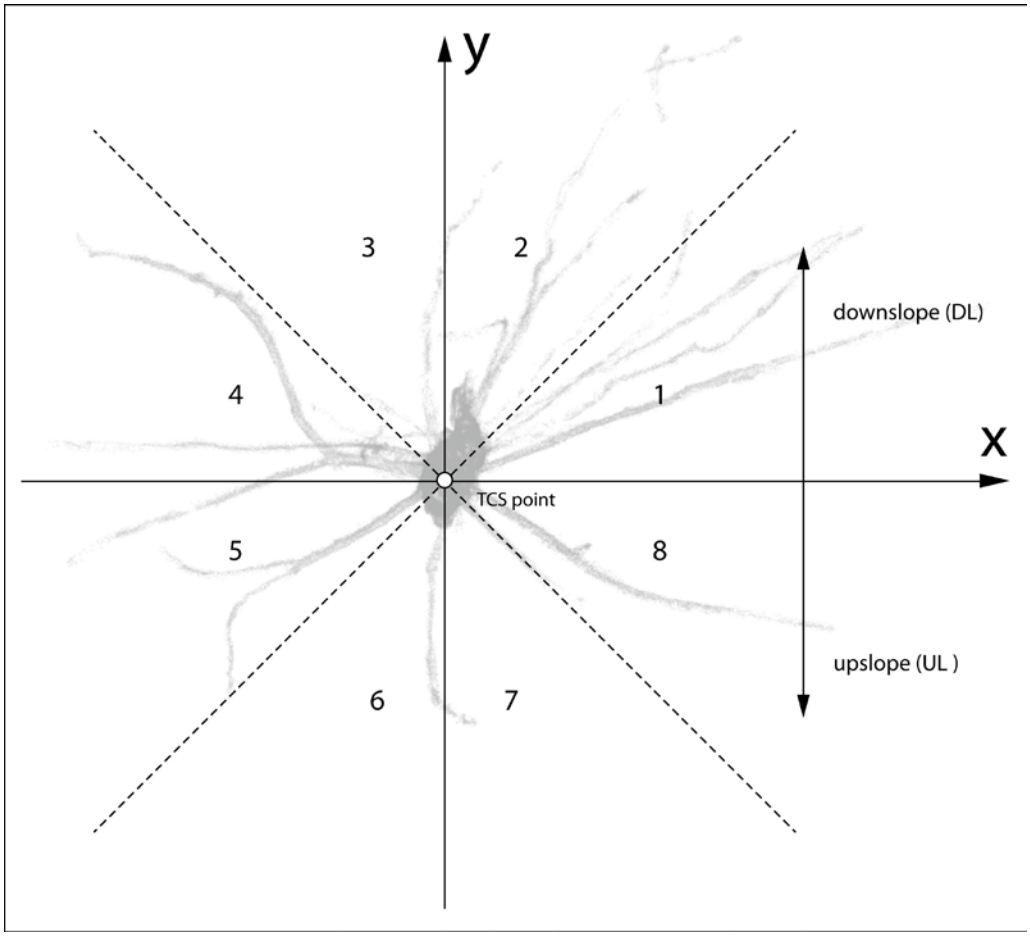

Figure 2.4.3. Orientation of the tree root system; from the bird's eye view; x-axis is parallel to the levee line, and y-axis is normal to the x-axis. A positive y-value denotes the downslope levee (DL) side, whereas a negative value denotes the upslope side. The origin is the TCS point. The parallel to levee zone (PRL zone) is marked by sectors 1, 4, 5, and 8; the perpendicular to levee zone (PDL zone) is marked by sectors 2, 3, 6, and 7. The XR (right side) zone is marked by sectors 1, 2, 7, and 8; the XL (left side) zone is marked by sectors 3, 4, 5, and 6. X = X axis.

Root number (RN). In the PRL zone, RN was compared by using the levee slope line as the axis of symmetry, i.e., RN in the no. 1 and 8 sectors vs. in the no. 4 and

5 sectors). In the PDL zone, RN was compared by using the levee line as the axis of symmetry, i.e., RN in the no. 2 and 3 sectors vs. in the no. 6 and 7 sectors).

Root biomass distribution. The root biomass distribution was also used to evaluate the symmetrical/asymmetrical distribution of root biomass. The levee line and slope line were used as two axes of symmetry. In the upslope vs. the downslope directions, root system extent was compared, measured from the TCS point, expressed in terms of decreasing biomass, using tomographic slices with spherical coordinates (RCSA), as illustrated in Fig. 2.3.3.3. In addition, by setting the levee slope line as the axis of symmetry, root system extent was compared in the no. 1, 2, 7, 8 sectors (XR zone) vs. in the no. 3, 4, 5, 6 sectors (XL zone). The following statistical model was developed.

$$Y_i = ß_0 + ß_1 X_i + ß_2 X_i 1(X_i) + \varepsilon_i, \; i = 1, 2, \ldots, 50 \qquad (1)$$

where:

Y_i is the natural logarithm of the RCSA/slice of the *i*th tomographic slice

ß is a coefficient determining the contribution of the associated variable

X_i is the *i*th tomographic slice's horizontal distance to the TCS point

$1(X_i)$ is an indicator function defined as:

To compare the upslope/downslope distribution, $1(X_i) = 1$, if X_i is downslope; $1(X_i) = 0$, if X_i is upslope. To compare the root biomass distribution parallel to the levee line, $1(X_i) = 1$, if X_i is XL zone; $1(X_i) = 0$, if X_i is XR zone.

ε_i is the random error associated with the *i*th tomographic slice

Here we assume that ε_i independently follows normal distribution with standard parameters (mean 0 and standard deviation 1).

III. RESULTS

Two oak tree root systems were excavated on the Pocket levee, and imaged with ground-based T-LiDAR as described in the Methods; one of the two oaks was used extensively as a basis for methods development. The root system of that tree is shown in Appendix 1, with a photograph and the corresponding LiDAR image; and in an image assembly with the soil surface and aboveground part of the tree.

Similarly, valley oaks and cottonwoods were excavated at the Vernalis site. The field excavation and LiDAR imaging process are shown in Appendix 2. A final image assembly of one of the excavated cottonwoods based on the LiDAR data, including the root system, the soil surface, and the aboveground part of the tree, is shown in Appendix 3.

3.1 Upslope/Downslope Root System Asymmetry

Root biomass distribution. Tree root systems along the levee slope showed a general pattern of upslope vs. downslope asymmetry in biomass distribution (table 3.1.1). The root biomass in most root systems exponentially decreased from the TCS point in both upslope and downslope directions ($P < 0.05$), both in the Pocket levee and the Vernalis levee. Secondly, in general the root biomass distribution in the upslope direction had a significantly higher rate of decrease, from the TCS point to the maximum extent of the root system, compared to the downslope side.

Only two exceptions were observed, tree root system v13 and v16. Both showed the opposite trend, that root biomass decreased more rapidly in the downslope side than in the upslope side. Tree v13 grew in a site with a disturbed condition (flooding event in its first year). Tree v16 was not a well-developed tree root system with only four major roots.

Species differences: cottonwood vs. valley oak. The cottonwood trees had a comparatively higher woody root biomass closer to the trunk, and a lower decreasing rate of biomass distribution than the valley oak trees, either in the upslope or downslope direction. This means that cottonwood trees had proportionately more-extensive root systems than oaks, taking into account the differences in tree size among the samples.

Table 3.1.1 Decreasing rate of biomass distribution of the upslope (RBDu) and downslope (RBDd) side. Data include Vernalis trees and one oak from Pocket levee.

Tree ID	v6	v7	v8	v9	v12	v13	v14	v15	v16	v17	v19	v20	v21	v22	v23	p2009
RBDu	-2.67	-10.28	-8.08	-7.46	-4.01	-2.68	-6.64	-3.55	-0.78	-5.83	-4.33	-3.62	-7.02	-4.15	-4.44	-1.78
RBDd	-1.68	-1.28	-4.36	-3.38	-1.24	-3.55	-3.51	-2.66	-3.65	-2.99	-3.23	-1.96	-5.57	-2.74	-3.96	-1.36

Root number counts (table 3.1.2) also demonstrated an upslope/downslope asymmetry in most root systems, measured using the levee line as the X-axis of symmetry, and dividing into upslope-downslope (perpendicular to levee line, PDL), and XR-XL (right and left, parallel to the levee line, PRL). In general, there were fewer structural roots (the 2nd and 3rd order roots) in the upslope side than in the downslope side. The exceptions were tree root systems v16, v22 and v23 (table 3.1.3). Tree root system v16 was not well developed, as discussed above, with only 4 roots total. Even though the total biomass of trees 22 and 23 was greater in the downslope direction than upslope (see section above), the root number was higher in the upslope side.

There was no difference in general pattern of either biomass distribution or root number parallel to the X-axis (PRL), comparing the XR zone and XL zone. However, more structural roots grew along the PRL axis (table 3.1.4) compared with the PDL axis, a consistent configuration that can be seen in bird's-eye view in figure 4.3b. Tree root systems v9 and v22 were exceptions, with roots evenly distributed in all sectors. Both trees were growing close to a bigger tree; v9 was also closer to the levee toe than the other trees.

Table 3.1.2. Total root number in upslope/downslope sides. Vernalis trees and 1 Pocket oak.

Tree ID	v6	v8	v9	v12	v14	v15	v16	v17	v19	v21	v22	v23	p2009
Upslope	65	11	10	9	3	6	2	8	81	18	40	62	26
Downslope	187	27	42	52	21	31	2	21	97	22	17	66	74
All	252	38	52	61	24	37	4	29	178	40	57	128	100

Table 3.1.3. Root number of major structural roots (2nd and 3rd order roots) in upslope/downslope directions. Vernalis trees and 1 Pocket oak.

Tree ID	v6	v8	v9	v12	v14	v15	v16	v17	v19	v21	v22	v23	p2009
2nd order (upslope)	6	9	11	6	9	10	2	2	20	16	11	25	6
2nd order (downslope)	12	6	8	6	10	9	2	19	10	13	6	7	17
3rd order (upslope)	30	6	9	2	0	4	0	7	30	3	23	32	13
3rd order (downslope)	73	12	19	27	3	7	0	0	43	7	8	36	30
Upslope total	36	15	20	8	9	14	2	9	50	19	34	57	19
Downslope total	85	18	27	33	13	16	2	19	53	20	14	43	47

Table 3.1.4 Root number of major structural roots (2nd and 3rd order roots) in parallel (pRL) vs. perpendicular (PDL) zones. Vernalis trees and 1 Pocket oak.

Tree ID	v6	v8	v9	v12	v14	v15	v16	v17	v19	v21	v22	v23	p2009
2nd order (PRL)	13	6	7	9	12	12	3	12	22	18	9	17	18
2nd order (PDL)	5	9	12	3	7	7	1	9	8	11	8	15	5
3rd order (PRL)	66	13	15	16	2	7	0	6	42	7	12	43	23
3rd order (PDL)	37	5	13	13	1	4	0	1	31	3	19	25	20
PRL total	79	19	22	25	14	19	3	18	64	25	21	60	41
PDL total	42	14	25	16	8	11	1	10	39	14	27	40	25

3.2. Patterns of distribution of levee tree roots: shallow rooting pattern, vertical biomass distribution, and maximum rooting depth.

Tree root systems followed a generally lateral to oblique growth pattern with respect to the soil surface, both in upslope and downslope directions (figure 3.2.1), as determined by the rooting angle between roots and the slope surface. Horizontally-trending roots (defined as rooting angle of 0-30° with respect to slope angle) occupied over 70% of total root number in all trees except v19, which had about 58% of roots as horizontal roots.

Every root system excavated on the levees had a taproot. The two control trees, growing in the floodplain, both lacked a taproot. The maximum rooting depth, determined by the taproot length, ranged from 0.62 m to 2.61 m. The average rooting depth was almost one third of the maximum rooting depth, ranging from 0.36 m to 0.8 m (table 3.2.1). There was no statistical difference in average rooting depth between upslope vs. downslope directions (t-test, p-values non-significant).

In addition, in all root systems, 90% of cumulative biomass (DCB_{90}) was found between the soil surface and a depth ranging from 0.38 m to 1.55 m, i.e. no more than two-thirds of the maximum rooting depth. The Pocket oak, although larger and older than Vernalis oaks (mean age=35 in Pocket; mean age= 11 in Vernalis) had a biomass distribution by depth within the same range of values: 90% of cumulative biomass was found in upper 1.13m, with an MRD of 1.69 (data not shown). Therefore, DCB_{90}/MRD of the Pocket oak = 66.9%, two-thirds of the maximum rooting depth, as observed in Vernalis. Together these results – lateral root angle, and cumulative biomass - demonstrate a highly consistent, and shallow lateral distribution pattern of the tree root systems along the levee slopes in relation to the soil surface (shown also in Figure 3.2.1). This shallow pattern of lateral root distribution was consistent regardless of tree size (see 3.3.1 below).

Table 3.2.1. Rooting depth (m). Vernalis trees.

Tree ID	v6	v7	v8	v9	v12	v13	v14	v15	v16	v17	v19	v20	v21	v22	v23
DBH (m)	0.24	0.36	0.15	0.17	0.22	0.11	0.13	0.12	0.08	0.13	0.22	0.16	0.13	0.16	0.21
Average rooting depth (ARD)	0.47	0.8	0.58	0.51	0.47	0.46	0.4	0.43	0.36	0.46	0.57	0.46	0.66	0.71	0.69
Maximum rooting depth (with taproot) (MRD)	1.7	2.61	1.45	1.88	1.36	1.03	1.27	1.09	0.62	1.56	1.89	1.34	2.01	1.89	1.91
ARD/MRD Ratio	28%	31%	40%	27%	35%	45%	31%	39%	58%	29%	30%	34%	33%	38%	36%
Depth of 90% cumulative biomass (DCB_{90})	0.83	1.55	0.88	1.14	0.95	0.72	0.83	0.66	0.38	1.09	1.23	0.87	0.87	1.15	1.24
DCB_{90}/MRD Ratio	49%	59%	61%	61%	70%	70%	65%	61%	61%	70%	65%	65%	43%	61%	65%

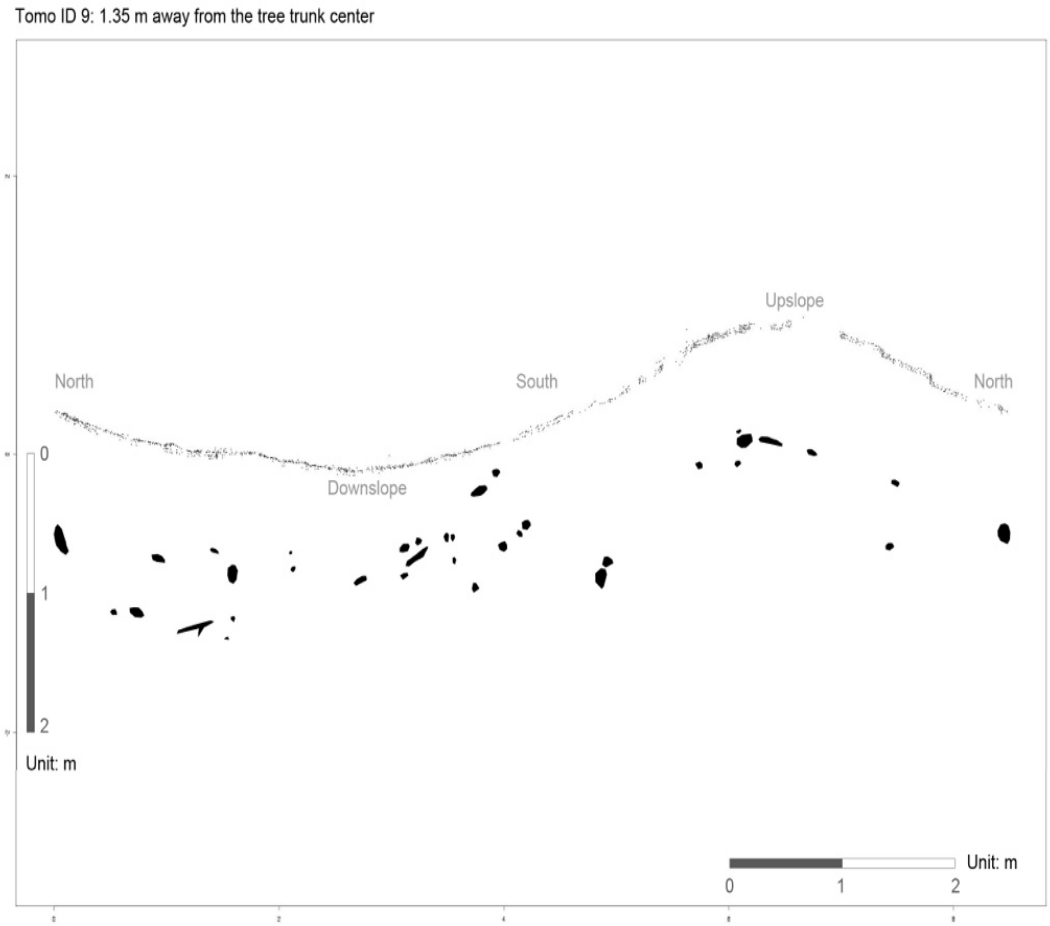

Figure 3.2.1. Shallow lateral growth pattern of tree root systems, illustrated in this slice of the Pocket oak root system (tree is 35 years old), using spherical coordinates (Tree ID: p2009; tomo ID: 9; 1.35m away from the tree trunk center).

3.3 Correlating Aboveground Values (DBH) with Belowground Patterns

We pursued the hypothesis that stem diameter (DBH) will scale with measures of belowground biomass, with the possibility of being used as a proxy measurement. The aboveground/belowground allometric balance could provide an easy and non-destructive

way to estimate belowground biomass. Rooting depth (section 3.3.1), horizontal extent (section 3.3.2), and root system branching pattern (section 3.3.3) were used as the belowground response variables.

3.3.1 DBH and rooting depth

Rooting depth was measured as: average rooting depth (ARD), maximum rooting depth (MRD), and depth of 90% root biomass (DCB90), shown in Figure 3.3.1. The tree root systems consisted of both a taproot and laterally-growing structural roots; it could be hypothesized that the depth of the taproot could correlate with DBH, whereas the depth of the lateral structural roots, might not, thus indicating that trees maintain a relatively shallow lateral root system with time. To test this hypothesis, we compared the linear regression of DBH vs ARD with taproot included (Figure 3.3.1.1), with DBH vs ARD but omitting the taproot (Figures 3.3.1.4).

The average rooting depth (ARD) when the taproot was included showed a positive but weak correlation with DBH (R^2 = 0.38981) (figure 3.3.1.1). Both the maximum rooting depth (MRD) and DCB_{90} had stronger positive correlations with DBH (R^2 = 0.59174 and 0.5983, respectively) than ARD (figure 3.3.1.2). By contrast, when the taproot was omitted from rooting depth calculations, the ARD had a very weak correlation with DBH (R^2 = 0.1301, Fig. 3.3.1.4). Therefore, it must be emphasized that although the taproot depth correlates with DBH, as indicated by R^2 values in Figure 3.3.1.1, 3.3.1.2, and 3.3.1.3, nevertheless, most of the variation in the depth of the lateral structural roots must be attributed to factors other than tree size as measured by DBH.

Figure 3.3.1. Linear regressions for DBH and root biomass. 1) DBH vs. average rooting depth; 2) DBH vs. maximum rooting depth; 3) DBH vs. depth of 90% cumulative biomass. 4) DBH vs. average rooting depth, omitting the taproot. All calculations based on Vernalis data.

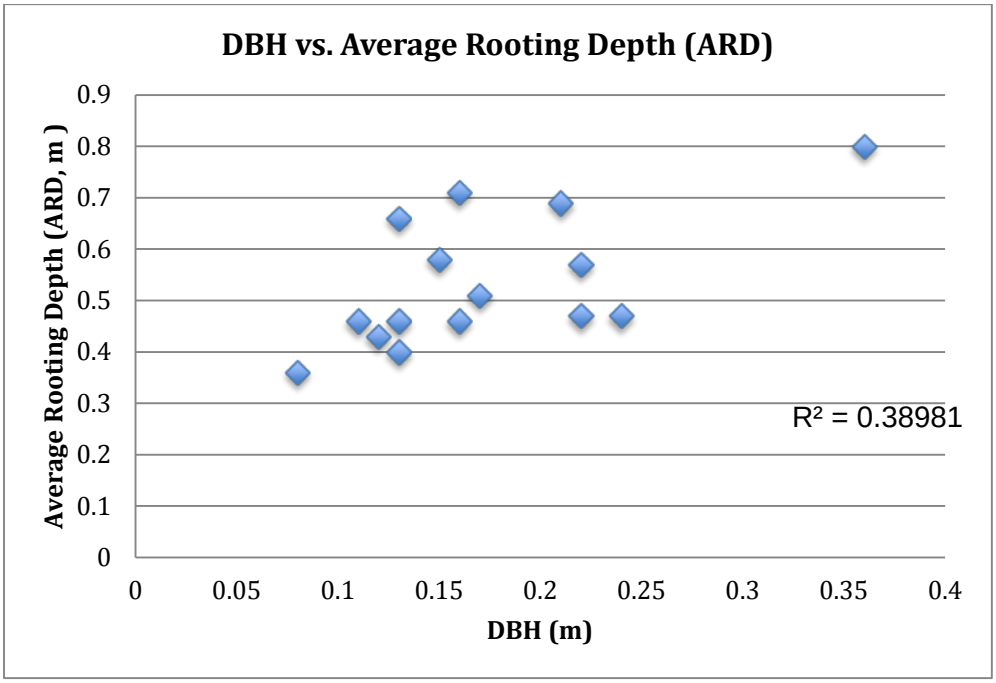

3.3.1.1

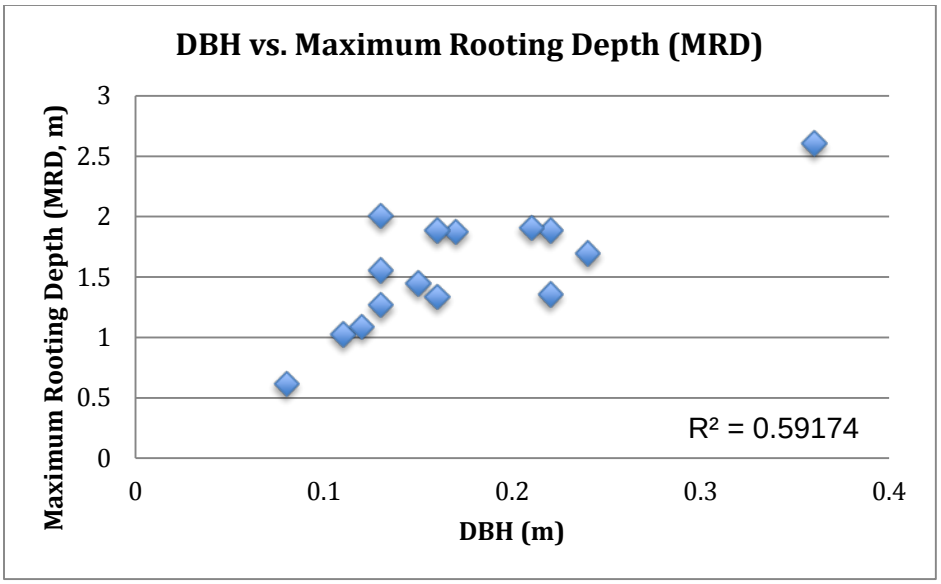
DBH vs. Maximum Rooting Depth (MRD)
Maximum Rooting Depth (MRD, m)
3
2.5
2
1.5
1
0.5
0
0
0.1
0.2
0.3
0.4
DBH (m)
R² = 0.59174

3.3.1.2

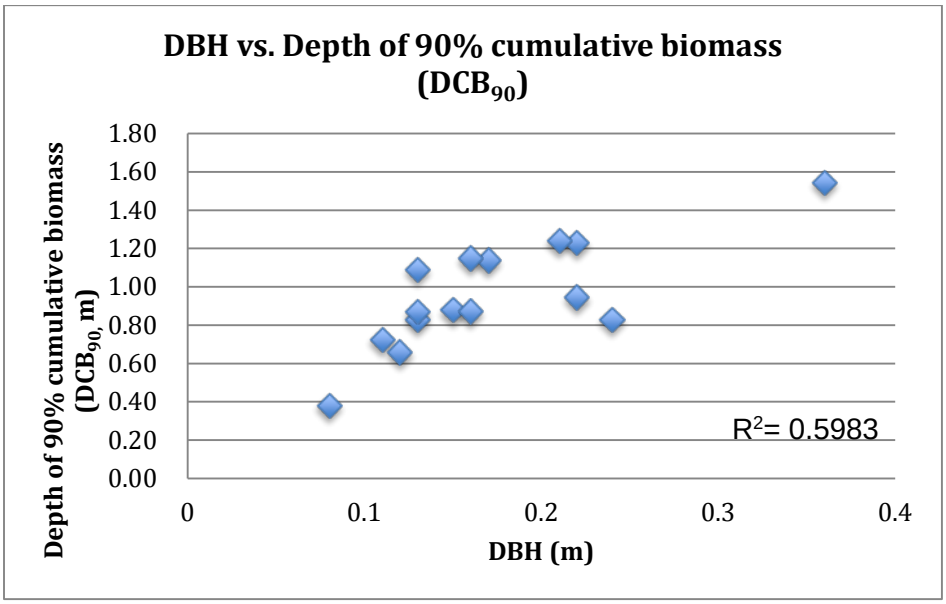
DBH vs. Depth of 90% cumulative biomass (DCB90)
Depth of 90% cumulative biomass (DCB90, m)
1.80
1.60
1.40
1.20
1.00
0.80
0.60
0.40
0.20
0.00
0
0.1
0.2
0.3
0.4
DBH (m)
R2= 0.5983

3.3.1.3

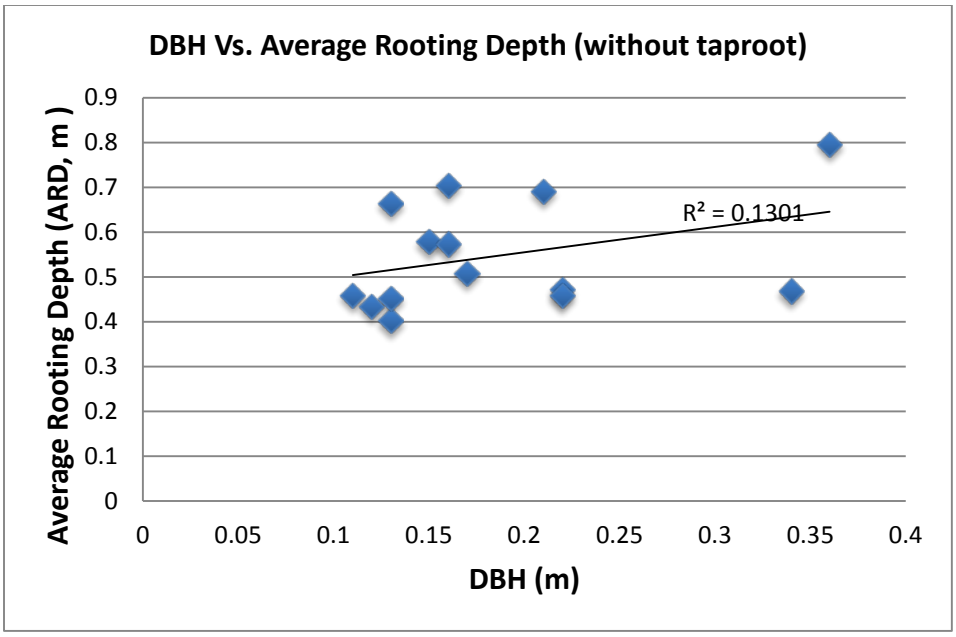

3.3.1.4

3.3.2 DBH and root system horizontal extent

Tree DBH was strongly positively correlated with root maximum extent (figure 3.3.2). However, the downslope root maximum extent had a stronger positive correlation with DBH than upslope (figure 3.3.2). This indicates that the difference between upslope and downslope biomass accumulation is likely due to a restriction of root-system growth in the upslope direction of the levee.

Figure 3.3.2. Linear regressions for tree DBH and root-system horizontal extent. 1) DBH vs. maximum extent (all); 2) DBH vs. upslope root extent; and 3) DBH vs. downslope root extent.

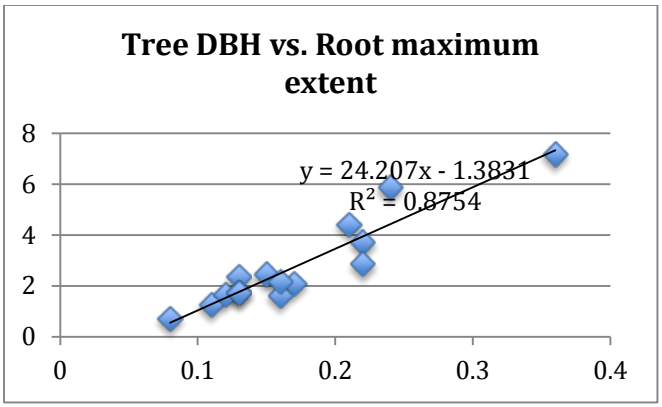
Tree DBH vs. Root maximum extent
y = 24.207x - 1.3831
R² = 0.8754
8
6
4
2
0
0
0.1
0.2
0.3
0.4

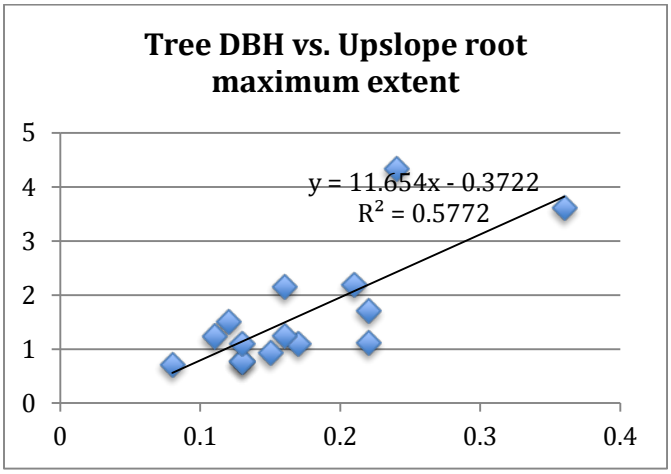
Tree DBH vs. Upslope root maximum extent
y = 11.654x - 0.3722
R² = 0.5772
5
4
3
2
1
0
0
0.1
0.2
0.3
0.4

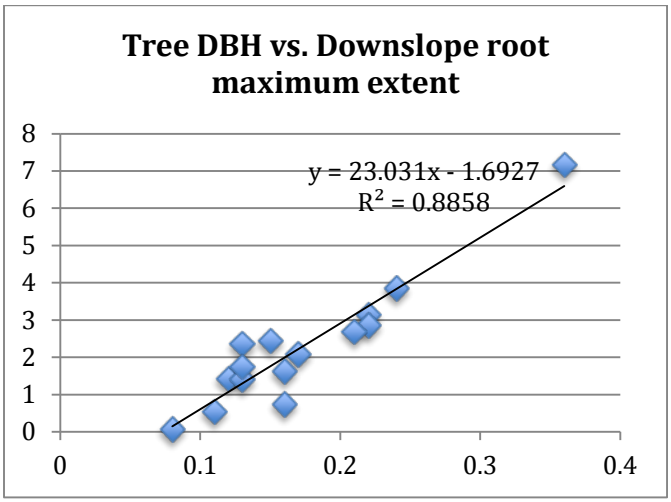
Tree DBH vs. Downslope root maximum extent
y = 23.031x - 1.6927
R² = 0.8858
8
7
6
5
4
3
2
1
0
0
0.1
0.2
0.3
0.4

3.4 Root Topological Index (root system branching pattern)

Quantitative characteristics that delineate the branching patterns of tree root systems were calculated using the topological indices (TI, table 3.4.1) as described in Oppelt et al. 2001. Topological indices range from 0 to 1, representing root system branching patterns from “dichotomous” to “herringbone”.

Table 3.4.1. Root system topological indices. Vernalis trees.

Tree ID	Overall TI	DBH (m)	Type
v6	0.0755	0.24	Dichotomous
v8	0.3701	0.15	Dichotomous
v9	0.3157	0.17	Dichotomous
v12	0.1579	0.22	Dichotomous
v14	0.7417	0.13	Herringbone
v15	0.5453	0.12	Herringbone
v16	1.0000	0.08	Herringbone
v17	0.6975	0.13	Herringbone
v19	0.1329	0.22	Dichotomous
v21	0.7031	0.13	Herringbone
v22	0.3213	0.16	Dichotomous
v23	0.2167	0.21	Dichotomous

3.4.2 DBH and topological index

Seven tree root systems were more “dichotomous” (TI < 0.5), while five were more “herringbone” (TI > 0.5); a highly significant pattern was revealed, however, by comparing branching pattern with DBH: topological indices decreased linearly with increasing tree DBH ($P < 0.001$) (figure 3.4.1). Smaller trees had a more “herringbone” branching pattern with higher topological index values, while bigger trees had a more

“dichotomous” root branching pattern with lower topological index values. Dichotomous branching is more biomechanically stable than a herringbone pattern (Oppelt et al. 2001).

Figure 3.4.1. Topological index against DBH from Vernalis data (table 3.4.1).

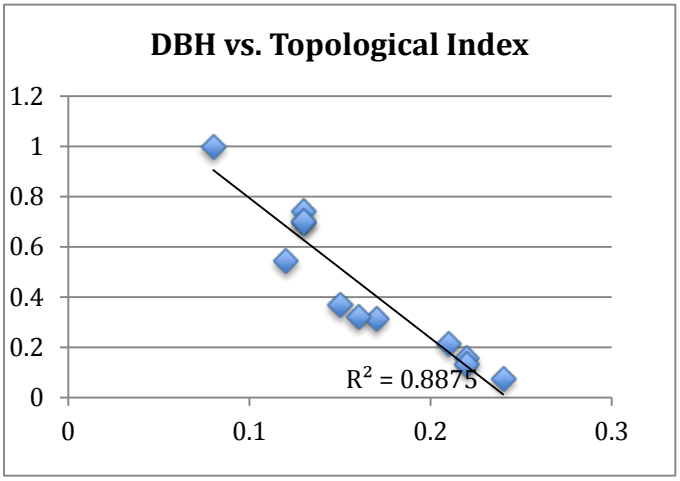

3.5. Rooting Patterns of a Mature Cottonwood in Clay-Soil Levee (Natomas East Main Drainage Canal)

We observed the following patterns of woody root distribution for the mature cottonwood on the levee slope, illustrated in Appendix 4 (photographs) and Appendix 5 (LiDAR image):

1) By and large, the woody roots exhibited a shallow and horizontal growing pattern.

2) The roots that were growing up into the levee showed a distinctive pattern of shallow horizontal growth for a distance from the trunk, followed by a step-like vertical downward

growth, but then the roots climbed upward again. It is likely that the vertical downward growth was related to cracks or other interfaces in the clay soil of the levee.

3) Although decay was noted in the major structural roots, no long channels were formed. There was some minimal cavity formation adjacent to the trunk, but it did not extent any appreciable distance into the roots.

3.6 Excavation of a Walnut Stump and Decaying Roots, Pocket Levee.

As seen in Appendix 6, a series of aerial images of the Pocket levee from 1993, 1998 and 2005 showed that the walnut tree had died and had been cut down sometime between 1993 and 1998; thus the root system had been subject to decay processes for at least 12 years before the excavation was carried out (2010). Careful excavation was carried out manually, revealing a thick (8”-12”) clay cap that had been laid down on the slope, probably as an erosion control measure (Dave Williams, CDWR, pers. comm.). Major roots were traced from the base of the stump until they disappeared in the soil, to an extent of 8’ in one case. As shown in Appendix 7, cavities were found at the base of the stump where roots had decayed completely, but only where the clay cap formed a roof over the cavity. When these roots were traced away from the stump, the decayed portion appeared as a somewhat darker color in the sandy soil, indicative of organic matter. No channels were observed except as short cavities a few inches from the stump. When the whole remaining stump was lifted with a backhoe (Appendix 8), it could be seen that some major roots on the downslope face had a parallel orientation to the levee slope. On the upslope side, however, the roots were more vertical, and had a fused, flattened appearance.

IV. DISCUSSION

4.1 Analytical Tools for Tree Root Systems

Because roots are buried in the soil, belowground patterns of root spatial distribution are still largely uncharacterized in accurate models. Our study provides a methodological pipeline that combines a series of accessible analytical tools for *in situ* tree root system characterization.

First, we have utilized a simple yet high-resolution data format (3D .xyz format) for processing tree root system data acquired by terrestrial LiDAR scanning, that can be adapted in commonly used spatial analysis programs.

Secondly, we have built two fundamental quantitative models (biomass and vector) for quantitative analysis that enable the posing and answering of higher-order questions about root systems.

1. LiDAR scanning of tree root systems

Potential applications of imaging pneumatically-excavated tree root systems using T-LiDAR derive from the high-resolution, 3D nature of the imaging system combined with *in situ* spatial preservation, which we have used as a basis for quantitative analysis. Teobaldelli et al. (2007) assembled T-LiDAR scans of aboveground features, soil surface, and root systems, but did not carry out quantitative analysis. T-LiDAR was demonstrated to acquire high resolution images of individual tree roots (Gärtner et al. 2009), but spatial relationships of root systems with soil were not determined, since the tree roots were not imaged *in situ*. In previous analyses of *in situ* tree root distribution patterns, a hand-digitizer (Polhemus) was used to reconstruct root

volumes and directionality with digital surface trace lines (Danjon et al.(2005, Danjon and Reubens 2008. The hand-digitizer is not able to acquire slope surface data on the scale of a tree root system.

At the data processing stage, the LiDARViewer tool (Kreylos *et al.*, 2008) with 3D visualization environment (3D display) can be used for high accuracy of 3D spatial simulations of tree root systems (Figure 2c). One of the major problems encountered with LiDAR point cloud data of tree roots is the presence of soil, or crossing roots, which create image noise. Using LiDARViewer with 3D goggles (e.g., complementary color anaglyphs) one can easily create a 3D visualization environment on any common computer monitor. When accompanied by photographic documentation taken during the excavation of the root system, data clean-up for noise reduction can be readily achieved.

The final product is a point-cloud data set in .xyz format. At the data analysis stage, our biomass or vector models can be created in any CAD (computer-aided design) software, imported into or plotted on any GIS or R program, and exported as data tables in common file types, such as ASCII, CSV, or Excel spreadsheet for spatial, geometric, or topological analysis.

2. Building biomass and vector models from T-LiDAR data.

The ease and accuracy of digital processing enables the building of highly accurate reconstructions and models. Two key biological parameters (e.g., root area ratio and penetrating angle) play critical roles in slope failure processes (Stokes *et al.*, 2008), and we used these parameters as a basis for model-building in our analyses (biomass model and vector model).

T-LiDAR based models have the potential to be further applied in solving a range of problems related to root architecture and tree stability, and belowground carbon storage, at different spatial or temporal scales. The center of origin of the trunk and root system (TCS point) can be accurately defined within a biologically consistent reference system that can take into account cumulative changes that correspond to scales greater than one year, e.g. modeling belowground biomass distribution patterns over time, based on tree samples of different sizes; or correlation with other tree growth parameters such as DBH. The 3D data for aboveground parts of tree biomass, geomorphology of slope surface, and the belowground root biomass can be combined; and by extension from the parametric approaches such as those described in this report, applicability can extend to areas of investigation that have been impossible to explore systematically previously.

Parameters such as root volume can be retrieved from the analysis of root geometry, for estimates of belowground carbon-storage. Based on the current-generation imaging capabilities of T-LiDAR, the estimation of tree root biomass can potentially be scaled from a single root to a forest ecosystem. Moreover, in combination with remote sensing by aerial LiDAR imaging (Lefsky *et al.*, 2005), the models and resulting databases have the potential to contribute to a precise and efficient hierarchical approach to estimate forest productivity, or to reconstruct spatial configurations in the rhizosphere, or, as mentioned above, to evaluate carbon sequestration processes at several scales.

4.2 Taproot Type Architecture

Biomechanical forces generated by slopes are a major influence on woody-root architecture in several respects. In the trees excavated in this study, the root systems on the levee slopes uniformly developed taproots, whereas trees growing in the floodplain had no taproots. Tree root systems have been reported to develop specific patterns in response to different anchorage conditions corresponding to slope angles: on the flat (< 4°), shallow slopes (< 10°), and steeper slopes (> 10°) (Chiatante *et al.*, 2003; Sun *et al.*, 2008). Taproots may occur on steeper slopes (Soethe *et al.*, 2006; Sun *et al.*, 2008), but are rarely present on the flat or shallow slopes (Ghani *et al.*, 2009). Taproot emergence in a tree root system thus correlates with the tree's anchorage mechanisms in response to asymmetricl biomechanical forces. Other factors may be involved in determining the presence or absence of a taproot for a given species. Gale and Grigal (1987) noted genetic differences in rooting patterns based on successional adaptation; moreover, they cite an earlier report (Wagg 1967) that for *Picea glauca*, taproots formed in well-drained soils, but not in soils with high moisture content.

In addition to the presence of a taproot, it has been reported that root systems on slopes have a higher lateral branching rate of lateral structural roots close to the soil surface (Chiatante et al. 2003), that can dissipate forces and self-loading from the aboveground compartments (Di Iorio *et al.*, 2005). These second-order structural roots are either horizontal or oblique branches. Our results support this conclusion, demonstrating a horizontal and shallow growth pattern of lateral structural roots of the trees excavated on slopes of two levees. Consequently, root systems adapted to slopes >10º develop a dimorphic architecture, i.e. an "umbrella" or cone-shaped architecture, consisting of a taproot with spreading, shallow lateral structural roots (Figure 4.3 a). The growth pattern of the tree roots on levees reflects this pattern: levee tree root systems had 90% of the root biomass in the upper 1 m in most cases.

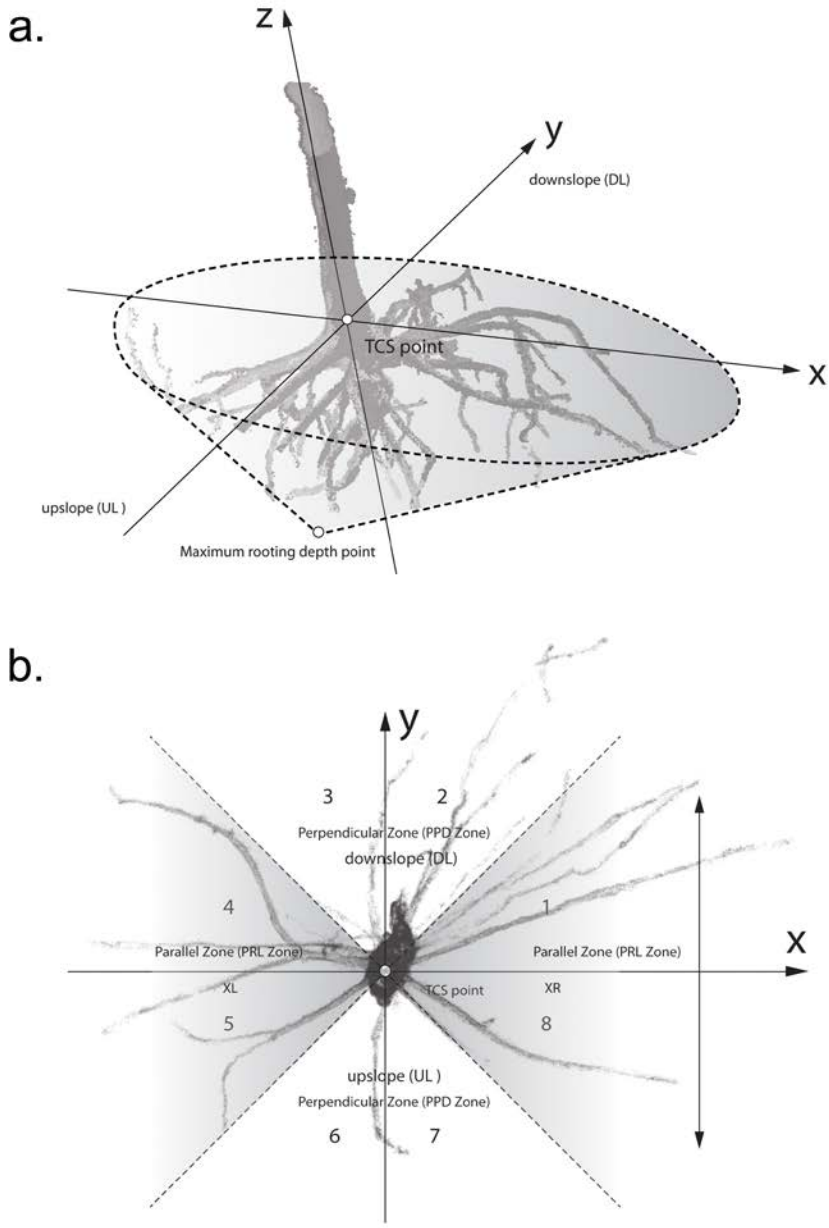

Figure 4.3 (a) The 3D perspective of the “umbrella/cone” shape of tree root architecture (TreeID: v08); (b) The 2D perspective from the bird’s eye view of the “spider” shape of tree root architecture.

4.3 Comparison of the upslope/downslope asymmetry between levee slopes and other types of slopes

The asymmetrical distribution of root biomass along upslope/downslope direction in the levee system was strikingly different from what has been reported for other slopes, in that there was generally a much lower root biomass on the upslope side of the trees growing on the levee slopes. Although the levee root systems had a dimorphic architecture with a taproot, the center of mass or volume was not located on the upslope but rather on the downslope side. Total root biomass was higher on the downslope side of the tree. Additionally, root systems on levees showed a higher decreasing rate of biomass distribution on the upslope side.

By contrast, on other slopes, it has been found that woody perennials have more root biomass on the upslope side than the downslope side, and an uneven upslope/downslope distribution of sub-order lateral roots (Chiatante *et al.*, 2003). Total volume of all roots (except for the tap root), number and length of the second order roots are typically higher in the upslope side than in the downslope side; and larger lateral roots are also more abundant (Chiatante *et al.*, 2003; Di Iorio *et al.*, 2005). Roots on the upslope side have been shown to have a higher stiffness than those extending downhill (Di Iorio *et al.*, 2005; Sun *et al.*, 2008). Resistance to aboveground weight asymmetry likely causes the uneven biomass distribution patterns, which act functionally to prevent pullout uprooting (Di Iorio *et al.*, 2005).

Moreover, our findings indicate that upslope/downslope asymmetry is most likely due to inhibition of root growth in the upslope direction, and not promotion of growth in the downslope direction. Tree root systems adapt to the levee slope and likely develop different rooting patterns compared with other slopes, due to the characteristics of the

levee geotechnical construction. The geotechnical composition of levee slopes is different from other non-engineered slopes from two perspectives. First, levee geometry is limited by the minimum prism criteria of levee height, slope angle, and crown width in most levee systems, including California levees (USACE Engineering Manual EM 1110-2-1913, 2000; USACE Sacramento District Geotechnical Levee Practice SOP, 2008). Compared to other slopes, therefore, the levee slope dimensions are limited or constrained, whereas the dimensions of other slopes are not *a priori* predictable. In addition, other slopes usually have a classical soil horizon profile, while levee slopes may have a more compact surface on the crown (upslope) and lower soil bulk density near the levee toe (downslope). The levees in this study were built from river sediment, with a soil particle composition either of a sand-to-sandy loam (Pocket levee) or a silt-sand loam (Vernalis levee). Moreover, in our study sites, a road with pavement 5 to 7 meters in width was constructed on compacted fill at the crown of the levee, to aid in levee inspection. Based on a limited replicated subset of soil measurements, the average soil bulk density in the upslope side was higher than the downslope side, either at the surface (1.46, SD=0.17 vs. 1.36, SD=0.23) or at the depth of over 1m (1.63, SD=0.28 vs. 1.49, SD=0.23); V. Claassen data, average of three tree sites in Vernalis). Critical bulk density for plant growth in a silt-sand soil corresponding to the particle composition measured in Vernalis is approximately 1.5 (Daddow & Warrington 1983). Thus the upslope/downslope asymmetry particular to these levee slopes may result from higher soil compaction of the upslope side and levee crown, impeding root system extension in that direction. Without more extensive soil characterization, it is equally possible that a difference in soil drainage or distance from the water table between the upslope and downslope directions in a system that experiences periods of high water or

inundation from the downslope direction, may influence the upslope/downslope asymmetry of root growth, since root growth is dependent on available soil water.

The inhibitory effect on upslope root system architecture may also explain the observed reinforcement of the root systems in the directions parallel to the levee, as a biomechanical compensation. In order to provide sufficient mechanical supports to tree stabilization on levees in the absence of upslope root-system reinforcement, levee tree root systems developed not only the umbrella/cone shape (Figure 4.3 a) but also the "spider-shape" architecture (Figure 4.3 b). From the bird's eye view, this architectural pattern consists of more lateral structural roots growing in the parallel zones than in the perpendicular zones. Robust growth of lateral structural roots transfers more self-loading force to the direction parallel to the levee line. In addition, it is necessary for the root systems to develop similar patterns in both directions along the parallel, so that loading force is evenly transferred to both sides of the root systems on the levee slope.

4.4 Implications of Above/belowground Relationships

Biomass distribution is highly controlled by soil interactions and is sensitive to environmental variations in water relations, soil physical characteristics, and nutrient supply on flat or shallow slopes (Henderson *et al.*, 1983; Fitter, 1988). As we observed, tree root system growth patterns and architecture on levees are strongly dominated by the slope.

The above/belowground allometric relationships can potentially provide simple, direct and non-destructive methods for approximation to reveal properties of tree root system architecture. The diameter at breast height (DBH) as a proxy for total

aboveground biomass has been reported as a predictor for root biomass estimation, using linear regression (Kuyah *et al.*, 2012). Our results for DBH vs. maximum rooting depth, and maximum extent of the tree root system confirm this finding, although not for the extent of the upslope portion of the root system. This suggests that growth in root length, both vertical and lateral, has a positive allometric relationship to aboveground biomass accumulation, except where root growth is limited by soil conditions. Importantly, however, while average rooting depth of the total dimorphic root system is proportional to DBH, the regression of average root depth of the lateral structural root system had an extremely low R^2 value.

Further, we show that DBH can be a predictor to estimate branching patterns (topological indices): In our study, larger trees had lower topological indices of root systems than smaller trees. However, we did not find any relationship between topological indices and measures of symmetry/asymmetry at a whole-tree scale. Instead, branching patterns of root systems more likely reflect environmental plasticity adapted to local conditions.

Implications of tree root architecture for tree stability on levees.

These findings show that roots continue to grow in length and accumulate biomass over time, including the taproot and the lateral structural roots. This architectural pattern confirms and extends the findings of Sobhani et al (2014), that root pit area of windthrow trees increases proportionally to DBH. By contrast, the depth of the lateral structural root system, which determines the depth of the potential root pit in a windthrow situation, does not keep increasing proportionately. On levee slopes, although there has been considerable speculation that the “divot” created by a large tree

will be proportionally deeper and more damaging than that of a smaller tree, this model is not supported by our data.

As an alternative, it could be inferred that a proportionally *shallower* root-pit could predispose larger trees to uproot in a windstorm compared with smaller trees, due to greater aboveground biomass, as modeled by Coutts (1983). At the same time, however, the presence of the taproot in the levee trees, that continues to grow in proportion to the aboveground biomass, would be expected to provide a strong stabilizing element, as described by Shields and Gray (1992).

With respect to topological index, increasing tree size (DBH) correlated with a significantly lower topological index corresponding to dichotomous branching. This branching pattern would be expected to result in increasingly greater stabilization of the root system (lower pullout potential) than a herringbone configuration (Oppelt *et al* 2001).

One of the major controversies in recent years, concerning the interaction of natural vegetation and man-made structures, has arisen in post-Hurricane Katrina assessment of levee safety. The understanding of the root architectural traits on levee slopes needs more scientific assessment and modeling of the impact of tree root systems on levee integrity and bank reinforcement, since it is a current critical issue in levee safety policy, nationally and internationally (Corcoran *et al.*, 2011). Our findings can provide a baseline for predicting tree root system patterns on sandy levees in the Central Valley of California. Additional studies of trees growing on levees in different soil conditions will be valuable to provide comparative findings.

VI. CONCLUSIONS

Tree root systems in levees in the Central Valley of California, including valley oaks and cottonwoods, were found to be dimorphic in architecture, and to have the following common architectural characteristics:

1) All of the trees growing on levee slopes had a strong vertical taproot, whereas trees growing in the floodplain did not.

2) Major woody lateral roots (>1" diameter) extended primarily in a horizontal or oblique orientation with respect to the soil surface.

3) Major woody lateral roots (>1" diameter) were located primarily (approximately 90% of total root biomass measured) in the upper 1-m of soil, and at a consistent depth regardless of direction (upslope, downslope, or parallel to the levee line).

4) There was a consistent pattern of biomass distribution, with decreasing biomass with increasing distance from the trunk center, regardless of direction.

5) However, the rate of biomass decrease was higher in the upslope direction, than in any other direction. That is, the root system was smaller in extent and the total root biomass was less in the upslope direction. This pattern is the reverse of patterns described for trees on other types of slopes, which have greater root biomass in the upslope direction (see Discussion). On levees with roads, soil

compaction likely influences the rooting pattern, but further soil sampling is needed to verify this possibility. Drainage properties of the sandy levees may also influence root distribution.

6) Interestingly, the major woody lateral roots extending parallel to the levee line in either direction had greater total biomass, greater root number and size, than comparable roots in either upslope or downslope directions. These patterns were independent of geospatial orientation of the levee lines in relation to cardinal directions, because the Pocket and Vernalis levees are oriented in different directions (in fact, the Vernalis trees were along a levee section that curved). The rooting patterns are thus most likely due to biomechanical interactions between the trees that were situated on the levee slopes and the levee structure, rather than to a directional climatic driver such as sun or prevailing wind. Since there is a reduction in upslope root growth, then a compensating biomechanical mechanism to accommodate asymmetric weight distribution of the trees, perhaps in response to differential compaction or some other type of soil physical property, that resulted in the observed strengthening of the roots parallel to the levee, would be a reasonable explanation.

7) Several belowground parameters correlated positively with DBH as a proxy for aboveground biomass, including maximum rooting depth, maximum horizontal extent of the root system, and weakly, average rooting depth of the dimorphic root system (taproot + lateral structural roots). However, average rooting depth of the lateral structural roots (minus the taproot) has a very weak correlation with DBH. Thus, belowground biomass accumulation would be expected to be proportional to aboveground biomass accumulation. However, the depth of the root plate does not increase in proportion to increasing DBH. These findings

provide confirming evidence for numerous casual or individual-tree observations of root plate architecture in scientific literature and arboricultural practice (e.g. Gasson & Cutler 1990), that lateral structural root plates of mature trees maintain a relatively shallow distributional pattern in relation to the soil surface, within approximately 1m of the soil surface.

ACKNOWLEDGMENTS

We greatly appreciate being part of the California Levee Vegetation Research Program. We are grateful for the outstanding support of the Sacramento Area Flood Control Agency (SAFCA), and California Department of Water Resources (DWR), both in funding the study and for innumerable logistical contributions. In addition, we recognize the invaluable assistance and contributions of numerous individuals from these and other organizations in facilitating and enabling our activities, notably Roy Kroll (DWR), and Mick Klasson (consultant to SAFCA), as well as DWR maintenance field staff on the Pocket Levee and from Reclamation District 1000. Eric Hopson of the US Fish & Wildlife Service gave us access to the Vernalis site in the San Joaquin River National Wildlife Refuge; Stephen Sheppard and others from River Partners provided essential field support at that site. Without all these individuals, and many more, we would not have been able to carry out the field operations. At UC Davis, Oliver Kreylos (W. M. Keck Center for Active Visualization in the Earth Sciences, UC Davis) provided advice in visualization, and Hannah Stone provided technical assistance; Victor Claassen (Department of Land, Air, Water Resources, UC Davis) contributed to the project in site management and soil analysis. Jeffrey Wu, Jaylee Tuil, Adam Akkari and numerous student assistants contributed greatly to our field operations.

REFERENCES

Chiatante D, Scippa SG, Di Iorio A, Sarnataro M. 2003. The influence of steep slopes on root system development. *Journal of plant growth regulation* **21**(4): 247-260.

Corcoran MK, Peters JF, Dunbar JB, Llopis JL, Tracy FT, Wibowo JL, Simms JE, Kees CE, McKay SK, Fischenich JC*, et al.* 2011. Initial Research into the Effects of Woody Vegetation on Levees.In: Headquarters, U.S. Army Corps of Engineers Washington, DC 20314-1000.

Daddow RL and Warrington JE. 1983. Growth-limiting soil bulk densities as influenced by soil texture. Watershed Systems Development Group, USDA Forest Service, Fort Collins, CO, WSDG-TN-00005.

Danjon, F., T. Fourcaud and D. Bert. 2005. Root architecture and wind-firmness of mature Pinus pinaster. New Phytologist. 168:387-400.

Danjon F, Reubens B. 2008. Assessing and analyzing 3D architecture of woody root systems, a review of methods and applications in tree and soil stability, resource acquisition and allocation. *Plant and Soil* **303**(1): 1-34.

Di Iorio A, Lasserre B, Scippa GS, Chiatante D. 2005. Root system architecture of Quercus pubescens trees growing on different sloping conditions. *Annals of Botany* **95**(2): 351-361.

Fitter A. 1988. Water relations of red clover Trifolium pratense L. as affected by VA mycorrhizal infection and phosphorus supply before and during drought. *Journal of Experimental Botany* **39**(5): 595-603.

Gale MR, Grigal DF. 1987. Vertical root distributions of northern tree species in relation to successional status. Canadian Journal of Forest Research, 1987, 17(8): 829-834.

Gasson PE & Cutler DF. 1990. Tree root plate morphology. The Arboricultural Journal14, 3: 193-264.

Gärtner, H., B. Wagner, I. Heinrich and C. Denier. 2009. 3D-laser scanning: a new method to analyze coarse tree root systems. Forest Snow and Landscape Research. 82:95-106.

Ghani MA, Stokes A, Fourcaud T. 2009. The effect of root architecture and root loss through trenching on the anchorage of tropical urban trees (Eugenia grandis Wight). *Trees-Structure and Function* **23**(2): 197-209.

Henderson R, Ford ED, Renshaw E, Deans J. 1983. Morphology of the structural root system of sitka spruce: analysis & quantitative description. *Forestry* **56**: 121-135.

Kreylos O, Bawden G, Kellogg L 2008. Immersive visualization and analysis of LiDAR data. In: Bebis G, Boyle R, Parvin B, Koracin D, Remagnino P, Porikli F, Peters J, Klosowski J, Arns L, Chun YK, Rhyne T-M, Monroe L, eds. *Advances in visual computing*. Berlin / Heidelberg, Germany: Springer, 846-855.

Kuyah S, Dietz J, Muthuri C, Jamnadass R, Mwangi P, Coe R, Neufeldt H. 2012. Allometric equations for estimating biomass in agricultural landscapes: II. Belowground biomass. *Agriculture, Ecosystems & Environment*.

Lefsky M, Turner D, Guzy M, Cohen W. 2005. Combining lidar estimates of aboveground biomass and Landsat estimates of stand age for spatially extensive validation of modeled forest productivity. *Remote Sensing of Environment* **95**(4): 549-558.

McGarigal, K., S. A. Cushman, M. C. Neel, and E. Ene. 2002. FRAGSTATS: Spatial Pattern Analysis Program for Categorical Maps. Computer software program

produced by the authors at the University of Massachusetts, Amherst. http://www.umass.edu/landeco/research/fragstats/fragstats.html

Oppelt AL, Kurth W, Godbold DL. 2001. Topology, scaling relations and Leonardo's rule in root systems from African tree species. *Tree Physiology* **21**(2-3): 117-128.

Reubens B, Poesen J, Danjon F, Geudens G, Muys B. 2007. The role of fine and coarse roots in shallow slope stability and soil erosion control with a focus on root system architecture: a review. *Trees-Structure and Function* **21**(4): 385-402.

Schuurman J, Goedewaagen M. 1965. *Methods for the examination of root systems and roots*. Wageningen, The Netherlands: Centre for Agricultural Publications and Documentation.

Shields FD and Gray DH. 1992. Effects of woody vegetation on sandy levee integrity. Water Resources Bulletin 28, 5: 917-931.

Soethe N, Lehmann J, Engels C. 2006. Root morphology and anchorage of six native tree species from a tropical montane forest and an elfin forest in Ecuador. *Plant and Soil* **279**(1): 173-185.

Stokes A, Norris JE, Beek LPH, Bogaard T, Cammeraat E, Mickovski SB, Jenner A, Iorio A, Fourcaud T 2008. How Vegetation Reinforces Soil on Slopes. In: Norris JE, Stokes A, Mickovski SB, Cammeraat E, Beek Rv, Nicoll BC, Achim A, eds. *Slope Stability and Erosion Control: Ecotechnological Solutions*. Dordrecht, The Netherlands: Springer, 65-118.

Sun HL, Li SC, Xiong WL, Yang ZR, Cui BS. 2008. Influence of slope on root system anchorage of *Pinus yunnanensis*. *Ecological engineering* **32**(1): 60-67.

Teobaldelli, M., T. Zenone, D. Puig, M. Matteucci, G. Seufert and V. Sequeira. 2007. Structural tree modelling of aboveground and belowground poplar tree using direct and indirect measurements: terrestrial laser scanning, WGROGRA, AMAPmod and JRC-3D ReconstructorÒ. Functional Structural Plant Models, Napier, New Zealand, November:4-9.

USACE Engineering Manual EM 1110-2-1913, Design and Construction of Levees. 2000.

USACE Sacramento District Geotechnical Levee Practice Standard Operating Procedures, REFP 10L0.doc 2008,

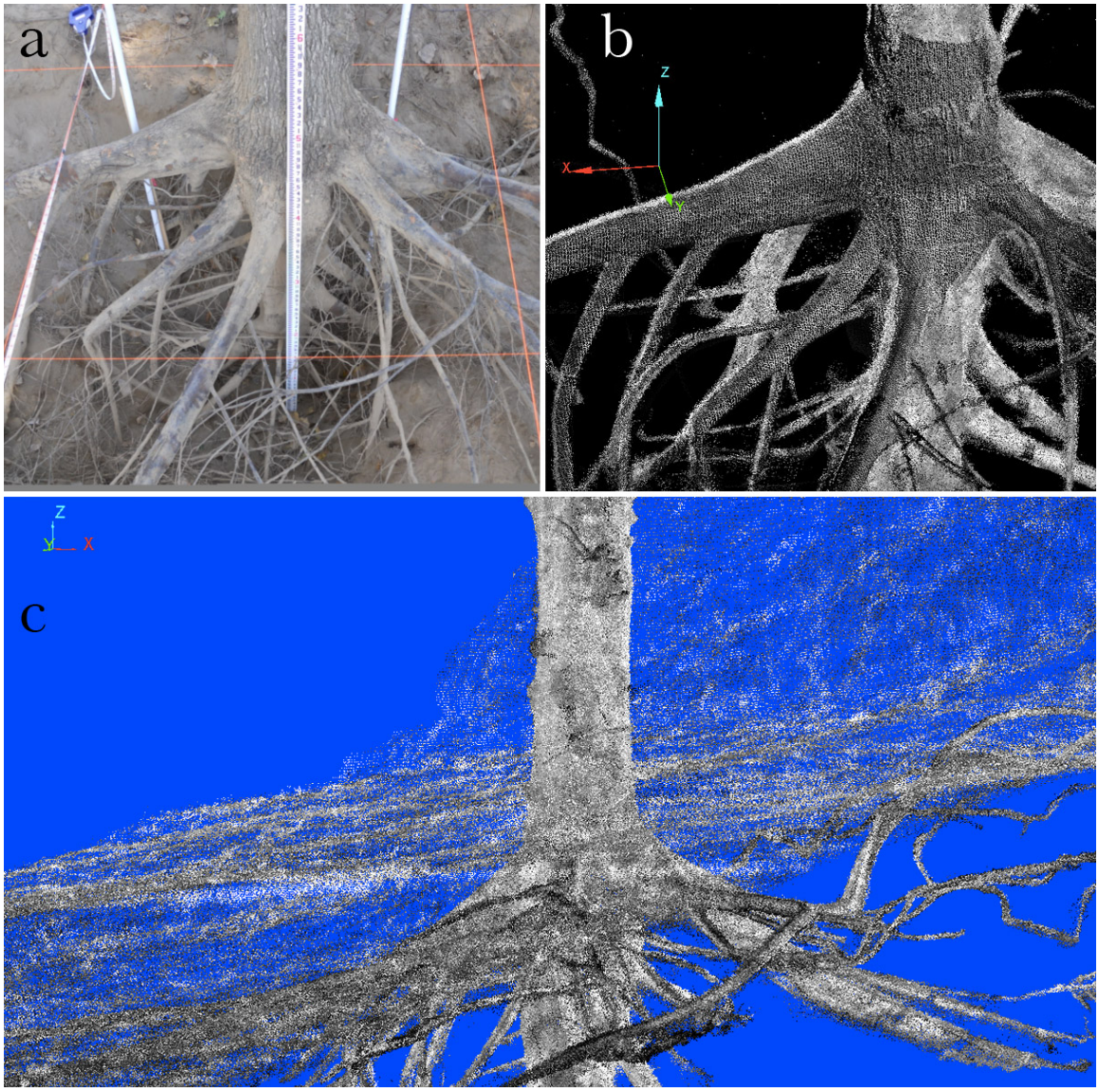

Appendix 1. Pocket oak tree root system after excavation. a) photograph; b) LiDAR image of the tree roots with the same orientation; and c) 3D reconstruction of the aboveground trunk, soil slope, and root system.

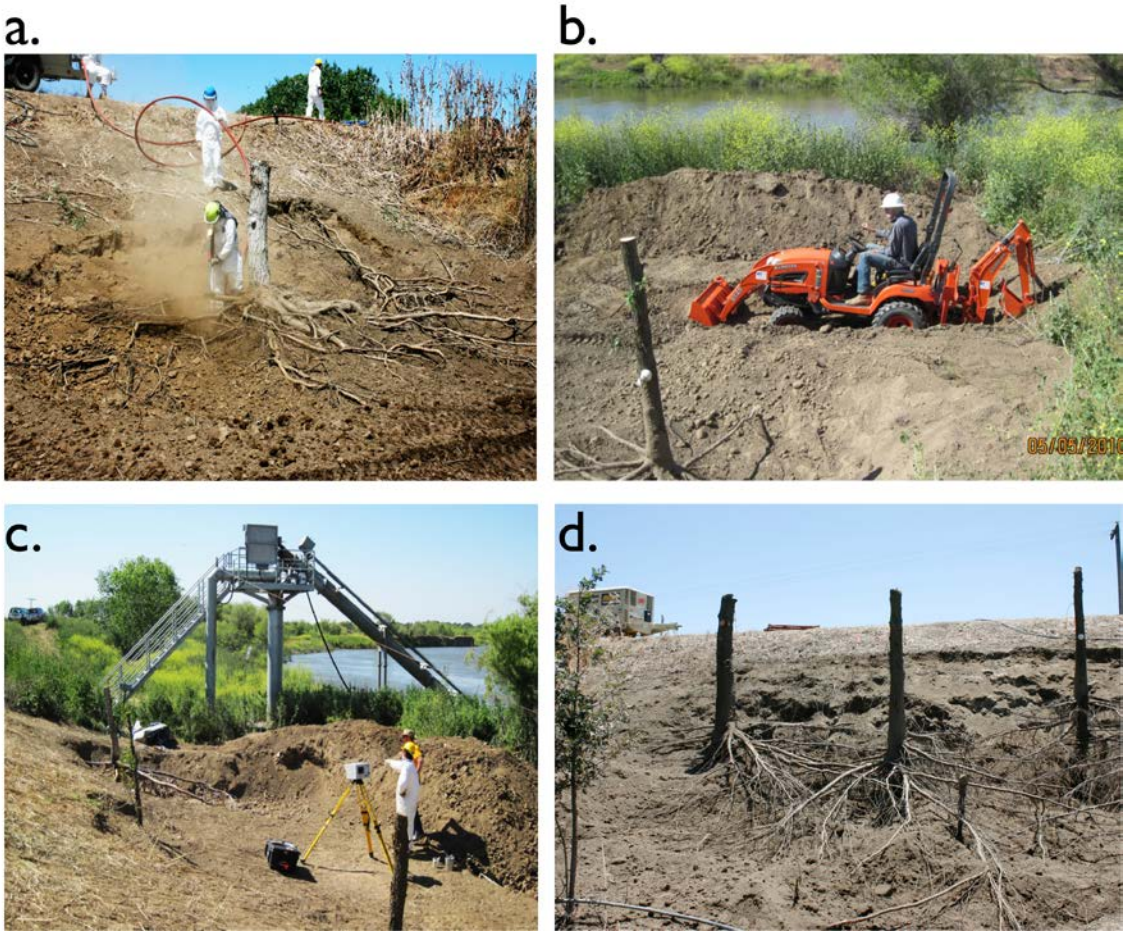

Appendix 2. Excavation and imaging process at the Vernalis site. A. Pneumatic excavation of tree root excavation. B. Soil removal and site clearance. C. Ground-based tripod LiDAR scanning. d) Several Valley oak trees after excavation.

Appendix 3. Three-dimensional reconstruction of a whole cottonwood tree with the actual *in situ* orientation of the root system with respect to the levee slope, using LiDAR imagery. Vernalis excavation site, tree ID v7.

Appendix 4. The mature cottonwood tree root system in the upslope direction. a). The root system has several major structural roots (maximum diameter: 0.8m; average diameter: 0.53m; minimum diameter: 0.16m; SD: 0.2). b). The extensive long root with smaller taper was parallel to the levee toward South. c). Large structural lateral root (A. Akkari standing on it) showed advanced decay, but no extensive hollow channels. d). Climbing roots with step-like growth pattern.

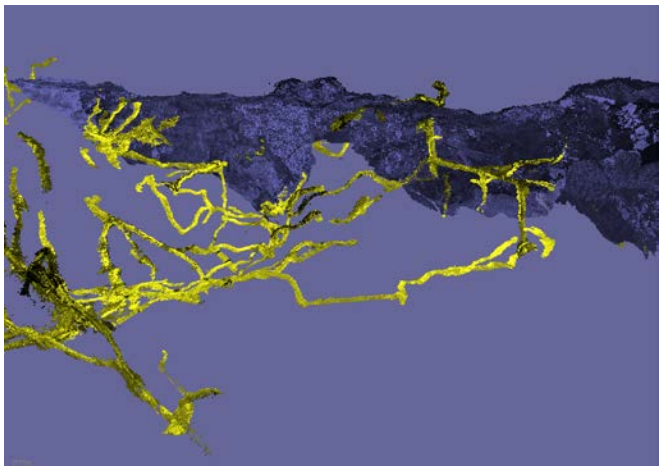

Appendix 5. LiDAR image showing climbing roots and a shallow growth pattern, scanned from below upwards, during mid-excavation. Some of the same roots can be seen also in Figure 1c, but photographed from above. However, the large, climbing root seen in Figure 1c had not yet been excavated when the LiDAR image was made.

Appendix 6. Walnut stump history. A row of relatively small walnut trees is evident in 1993 aerial photo (demarcated by small circles in the red bracket). But by 1998, two of the walnut trees had been removed. C) By 2005, the gaps in the original row where trees have been removed are evident. Therefore, the tree died and was cut down, between 12-15 years before it was excavated (2010).

Appendix 7. Walnut stump, Pocket levee. Manual excavation. A clay cap covered the sandy levee soil (red arrows, in A). Root “channels” were only formed at the interface of clay cap and sandy soil, at the base of the stump. These channels were short (visible in A). A major root was excavated with trowel and paintbrushes, in an advanced state of decay. Remaining wood is visible in B and C. No channels were observed leading away from the stump. Instead, sand filled in as roots decayed (D). A darker color of sand was observable where the roots had been, indicating organic matter.

A

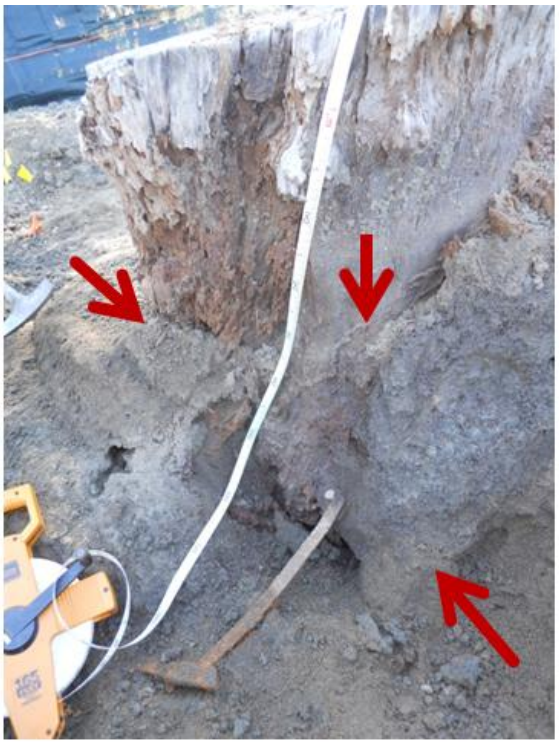

B

C

D

Appendix 8. Walnut stump excavated with a backhoe, Pocket levee. A. Several major horizontally-growing roots were oriented parallel to the slope (arrow). B. Vertically-growing major structural roots occurred on the upslope side of the tree. C. Many of these upslope roots formed gnarly, burl-like structures.